SPIN: Synchronization Signal Based Positioning Algorithm for IoT Non-Terrestrial Networks

Vishnu Rajendran Chandrika, Jiayin Chen, *Member, IEEE*, Lutz Lampe, *Senior Member, IEEE*, Gus Vos, *Senior Member, IEEE*, and Serkan Dost

***Abstract*—Non-terrestrial networks (NTNs) complement the terrestrial cellular networks by extending coverage to the user equipments (UEs) located in unserved and underserved areas. One of the most critical problems faced by NTN UEs is the lack of uplink (UL) synchronization and the associated initial access failure resulting from the high Doppler frequency offset caused by satellite velocity. While NTN new radio (NR) UEs rely on global navigation satellite system (GNSS) to resolve the UL synchronization problem, it is not always feasible for power-critical NTN Internet-of-Things (IoT) UEs. To this end, we design Synchronization signal-based Positioning in IoT Non-terrestrial networks (SPIN) which enables the IoT UEs to tackle the UL synchronization problem. SPIN estimates position and velocity of the UE using time difference of arrival (TDOA) and frequency difference of arrival (FDOA) measurements on the downlink synchronization signals. Consequently, the UEs can use the position and velocity estimates to compute and compensate for the residual time and frequency offsets, thereby successfully synchronizing to the NTN uplink. We conduct physical layer and system level simulations to show the effectiveness of our solution. SPIN positioning accuracy achieves the Cramér-Rao lower bound and meets the target accuracy required for UL synchronization. We also compare the battery life of an NTN IoT UE which uses SPIN for UL synchronization with that of a UE using GNSS-based solution. Our numerical results show that SPIN has significant battery life savings over GNSS based solution while also maintaining a low computational complexity.**

***Index Terms*—NTN, NB-IoT, LTE-M, Positioning, TDOA, FDOA**

I. INTRODUCTION

NON-terrestrial network (NTN) refers to a network which involves satellites in low earth orbit (LEO), medium earth orbit (MEO), or geostationary earth orbit (GEO) or unmanned aircraft systems (UAS) enabling radio frequency communication between users [1]. In Release 17, the 3rd generation partnership project (3GPP) standardized the first phase of integration of conventional terrestrial cellular networks with NTN with an objective to achieve global cellular coverage. The 3GPP NTN standardization plan for Release 17 and beyond includes NTN support for new radio (NR) and Internet-of-Things (IoT) which covers both enhanced mobile broadband (eMBB) and massive machine type communications (mMTC) use cases. Cellular-NTN integration helps in extending the cellular communication service to currently unserved and underserved NR and IoT users which include those located in remote villages, aircrafts, ships, and cell-edge regions [2], [3]. While NTN use cases in eMBB mainly refer to high data rate applications such as broadband connectivity and media and entertainment, NTN-IoT use cases consider services such as wide and local area connectivities [2]. The wide area NTN IoT services include global connectivity between sensors and actuators scattered over a large geographical area, which are used in a variety of applications such as automotive and road transport, energy, and livestock management [4], [5]. On the other hand, local area IoT services provided by NTN encompass connectivity to sensors and actuators located in a smart grid system or a moving platform, e.g., a container on-board a vessel, a truck, or a train [2], [6].

In a cellular-NTN integrated network, the base station (BS) is present either on-board the satellite or on the earth connected to the satellite through a gateway. The main challenges faced by NTN communication are long propagation delay due to the large distance between satellite and user equipment (UE), significant difference in timing advance (TA) between UEs at different locations within the cell due to its large size, and huge Doppler shifts due to the movement of satellites. The large propagation delay results in stop-and-wait gaps in the bidirectional communication between the UE and the BS. On the other hand, the disparity of TAs between UEs situated at different locations in the cell results in a large overlap of uplink (UL) signals at the BS. Furthermore, the Doppler shift due to satellite velocity results in a high frequency offset in the UL signal at the BS. While the long propagation delay affects only the data rate of communication, TA disparity and Doppler shift directly impact the UL synchronization, thus making the network inaccessible to the UE. To solve the synchronization problem, 3GPP considers common TA and Doppler compensations with respect to a reference point (RP) in the cell. In addition, the working assumptions include global navigation satellite system (GNSS) capability in the UE. Thus, with the knowledge of its relative location with respect to the RP, the UE can compute and compensate for the residual TA and Doppler. The GNSS based solution is feasible for NR devices, whereas it is not always viable for IoT devices for several reasons including battery and cost constraints. While several state-of-the-art solutions are available to counter the NTN UL synchronization problem [7]–[10], a solution specifically tailored for IoT UEs which considers both the power constraints and the required accuracy is still

Vishnu Rajendran Chandrika, Jiayin Chen, and Lutz Lampe are with the Department of Electrical and Computer Engineering, The University of British Columbia, Vancouver, BC, Canada. Gus Vos and Serkan Dost are with Sierra Wireless Inc., Richmond, BC, Canada. Email: vishnurc@ece.ubc.ca, jiayinchen@ece.ubc.ca, lampe@ece.ubc.ca, gvos@sierrawireless.com, sdost@sierrawireless.com.

This work was supported by MITACS, Canada and Sierra Wireless, Inc.

unavailable. To this end, we design a positioning solution which utilizes the existing synchronization signals (SSs) in IoT NTN, and operates with minimal power consumption. In the following, we explain the motivation of our work by having a detailed discussion of the UL synchronization issues, GNSS based solution and its drawbacks, and the other state-of-the-art solutions, before listing the main contributions of our paper.

A. Motivation

1) UL Synchronization Problem: To partially solve the UL synchronization problem, 3GPP has agreed to enable the BS to compensate for the common TA and Doppler offset with respect to an RP in the cell [1]. While the BS pre-compensates the common TA and Doppler offset in DL, it post-compensates the common offsets on the received UL signal. During DL synchronization process, the UE estimates the sum of residual Doppler and local oscillator offset. However, unless the individual offset components are estimated, the UE cannot accurately pre-compensate for the residual Doppler. Likewise, for timing synchronization, the UE is unable to estimate accurate residual TA. Consequently, the UL signal suffers from large residual TA and Doppler shift depending on the location of the UE within the cell. For instance, if the RP is the cell center, the UEs located at the cell edge experience large residual Doppler and TA. Subsequently after DL synchronization, the UE tries to establish a connection with the network by initiating random access (RA) procedure, which involves the transmission of an RA preamble. However, the frequency offset due to the residual Doppler and the timing offset due to the residual TA will cause the preambles to remain undetected at the BS, resulting in connection establishment failure. It should be noted that the residual TA and Doppler offset are significantl high for LEO satellites while they are negligible for MEO or GEO satellites [11]. On the other hand, UAS experiences very low delay and Doppler which makes it similar or equivalent to a terrestrial network [1]. Therefore, we consider only LEO satellites in our design, analyses, and evaluation.

2) Need for UE Location: Since the network compensates common TA and Doppler offset with respect to an RP, the UE requires the knowledge of its own location, satellite location and velocity, and the coordinates of the RP to compute the residual offsets. To this end, 3GPP has decided to enable the network to broadcast the location coordinates of the RP and the ephemeris which consists of the position and velocity vectors of the satellite. In addition, 3GPP considers only those UEs with GNSS capability such that the UEs know their location and hence can compute and pre-compensate residual Doppler and TA. However, when battery-powered low-cost IoT UEs are considered, the assumption of GNSS capability poses several challenges which are discussed in the following.

3) GNSS Optimization Problem: 3GPP has recently agreed to allow UEs to have time gaps for the purpose of performing GNSS position fix The working assumptions for IoT NTN include UE incapability to perform GNSS and cellular operations simultaneously. Therefore, before the positioning time gaps, an IoT UE must terminate radio resource control (RRC) connected mode and transition to RRC idle mode to perform GNSS positioning. After obtaining the position fix the UE must re-establish connection which involves synchronization and RA procedures, thus resulting in huge battery drain. Consequently, for a battery-powered mobile IoT UE which occasionally changes its location, and has long connected modes, it is not feasible to rely on the GNSS assisted UL synchronization. In this regard, the 3GPP work item description (WID) document for NTN IoT Release 18 includes an item which is aimed at optimizing the GNSS operations involved in the UL synchronization procedure [12].

4) GNSS Unavailability Problem: Though 3GPP is currently focusing on IoT UEs with GNSS capability, there are many scenarios where GNSS is unavailable. First, GNSS chipset is not necessarily integrated into all cellular IoT devices for cost and battery impact reasons. Second, GNSS suffers from poor link budget due to long distance [13]. Consequently, GNSS fails even in outdoor scenarios with NLOS signals [14]. On the other hand, LEO satellites with antenna gains same as or more than that of GNSS, have better link budget [13][1]. Furthermore, GNSS signals are also highly susceptible to jamming and spoofin [8]. All the above problems result in GNSS unavailability which eventually leads to NTN communication failure in the UE.

5) Location-Based Services (LBS): There is a wide range of services which essentially require the UE's location, called LBS. Among them are emergency services, e.g., E911, and infotainment services such as map services, direction to a location, and local advertising [15, Ch. 1]. In terrestrial networks, UEs rely on GNSS, cellular positioning, or a hybrid of both to obtain the location. However, in an IoT NTN, these methods either do not work due to the lack of cellular coverage and the unavailability of GNSS or are not feasible due to UE power constraints. Alternatively, the focus on utilizing LEO communication satellites for LBS has been growing recently in light of the massive LEO constellations such as Starlink and Amazon-Kuiper [16].

To solve all the above discussed problems, we need a positioning solution as an alternative to GNSS which should be designed to specificall cater to the NTN-IoT requirements.

B. Related Work

To address the NTN UL synchronization problem during GNSS unavailability, a positioning solution using time difference of arrival (TDOA) measurements, is proposed in [7]. This method uses NR primary synchronization signals (PSS) from the serving LEO communication satellite to get the position fix However, this solution has several shortcomings. First, the method targets 5th generation (5G) NR UEs and hence cannot be directly adopted for NTN IoT standards such as long term evolution-MTC (LTE-M) or narrowband IoT (NB-IoT). For instance, when an NB-IoT UE uses narrowband primary synchronization signals (NPSS) and/or narrowband secondary synchronization signals (NSSS) in place of NR PSS, the

[1]This is not always true, since sometimes the LEO satellites may have lower antenna gains which results in a link budget similar to that of GNSS [1].

accuracy will be worse due to their smaller bandwidth. Second, the method directly uses the time of arrival (TOA) estimates obtained from the cellular synchronization step for positioning, which is limited by the sampling rate. Despite using a high sampling rate of 30.72 Msps in NR UEs, the achieved accuracy is found to be insuffic ent. D irectly a dopting t his s olution for NB-IoT and LTE-M UEs which use an acquisition sampling rate of 1.92 Msps makes it completely unfi f or U L synchronization purpose. Moreover, the method considers only NR PSS for which the accuracy could be improved by including NR secondary synchronization signal (SSS). The next problem is that the method uses unweighted least squares for solving the firs o rder T aylor s eries b ased l inearized e quations. I n an NTN network consisting of LEO satellites which move at a high velocity relative to the UE, the signal-to-noise ratio (SNR) of the received signal varies significantl o ver time. Under the highly varying SNR, a weighted least squares (WLS) solution undoubtedly gives better accuracy. Moreover, the solution does not utilize the frequency difference of arrival (FDOA) measurements which could significantl i mprove the position estimation [17]. Another pertinent problem with the method is that it uses beam center broadcast by the network as the initial location for the iterative positioning algorithm. However, we fin that the beam center for set-3 and set-4 satellites, the newly introduced satellite scenarios [18], can be very far from the true UE location. This may cause the positioning algorithm to wrongly converge to a local minimum. More importantly, this solution define o nly p osition acquisition which is performed before initiating an RRC connection. It does not defin a ny p osition t racking, w hich i s e ssential for maintaining the accuracy when the UE is mobile and stays in connected mode for long time. Finally, we also fin some shortcomings regarding the evaluation assumptions including the number of satellites, measurement noise model, and the UE location. The method considers only a single satellite for positioning which largely affects the achievable accuracy and the time taken to get a position fix I t t akes approximately 4.2 minutes to achieve a positioning accuracy of around 700 m. The achieved accuracy is insufficien f or t he p urpose o f UL synchronization in NTN especially when the synchronization error attributed by other sources, e.g., local oscillator offset, is high. In addition, the large positioning time results in high latency and huge energy consumption which are not feasible for an IoT UE. Currently planned and recently deployed LEO satellite constellations, e.g., Starlink [19], [20] and Amazon-Kuiper [20], are large such that the UEs may get visibility to several LEO communication satellites simultaneously or sequentially in a specifie d uration o f t ime. T herefore, the positioning solution and evaluation should consider a reference constellation which is a realistic scenario. Although a similar solution proposed in [21] takes the advantage of both TDOA and FDOA measurements, the evaluated positioning accuracy is not sufficien f or t he p urpose o f U L s ynchronization. Since their work aims to solve the TA estimation problem for NTN UEs, the required positioning accuracy is much less stringent than that of UL synchronization as discussed in Section II.

Another state-of-the-art solution for the UL synchronization problem is the network assisted closed-loop frequency and TA control [22]. This method can work even when the UE is in RRC connected mode. This is in contrast with the GNSS solution which cannot function simultaneously with cellular connected mode, especially in low-cost IoT devices. However, closed-loop control requires configuratio of measurement signals, e.g., sounding reference signal (SRS), and frequency and TA offset signaling via media access control (MAC) layer control element (CE) and/or downlink control information (DCI). In addition, closed-loop control can work only after the UL transmission of msg1 [23], which demands the support for enhanced physical random access channel (PRACH) formats and/or preambles [1]. The signaling overhead, the specificatio impact, and the requirement for enhanced PRACH make the closed-loop frequency and TA control an unfavorable choice.

Another solution recently introduced to tackle the UL synchronization problem during GNSS unavailability is to directly estimate the Doppler shift using the cellular reference signals transmitted at more than one frequency [8]. However, the method requires the network to transmit additional synchronization signal blocks (SSBs) at frequencies suffi iently far from that of the cell-definin SSB (CD-SSB). In addition, the network is also required to include indication of time and frequency locations of the additional SSB in the system information broadcast 1 (SIB1) associated with the CD-SSB. This signaling associated with the additional SSBs results in network overhead. Moreover, the SSB based solution is applicable only to NR UEs, and hence cannot be directly adopted to IoT UEs.

With an objective to design a positioning solution which solves the UL synchronization problem, it is worthwhile to study the cellular positioning techniques developed for terrestrial networks to determine if there are any solutions adoptable for NTNs. The currently standardized positioning methods for the terrestrial cellular networks mainly include observed time difference of arrival (OTDOA), uplink time difference of arrival (UTDOA), and enhanced cell ID (E-CID) [24]. While OTDOA is based on TDOA measured by the UE using the DL reference signals, UTDOA is based on the TDOA measured by the BS using the UL SRS. On the other hand, E-CID uses the geographical location of the BS as a rough estimate for the UE location, along with one or more additional measurements such as reference signal received power (RSRP), angle of arrival (AoA), TA, or round-trip time (RTT) to get a fine estimate. However, both AoA and UTDOA require UE to transmit SRS resulting in huge battery drain, which is not feasible for an IoT UE. On the other hand, RSRP based methods are very sensitive to the characteristics of the channel and hence provide poor accuracy. Furthermore, their positioning accuracy does not benefi from the signal characteristics such as duration and bandwidth [25]. More importantly, in all the above cellular positioning methods, the location server (LS) estimates the UE location using the measurements reported by either the UE or the BS [26]. Such solutions can operate only after the UE establishes an RRC connection with the network, and hence they cannot be used to solve the NTN UL synchronization issues. However, if self-positioning is performed by the UE using the TDOA measurements on DL broadcast signals, it could be used to solve the UL synchronization

problem. Similarly, the existing positioning solution for NR NTN [7] performs TDOA based self-positioning at the UE. To this end, inspired from both OTDOA and [7], we design SPIN, Synchronization signal-based Positioning in IoT Non-terrestrial networks, which performs TDOA measurements on the DL SSs, to enable self-positioning in an IoT UE. In contrast to the terrestrial network, the BSs in an NTN, i.e., the satellites, are moving, which results in varying Doppler shifts. Consequently, the UE experiences frequency differences between the DL signals received from one or more satellites at same or different time instants. Exploiting these additional measurements, we design SPIN such that the positioning algorithm includes both FDOA and TDOA measurements.

Thus, considering the shortcomings of the state-of-the-art solutions and the power constraints associated with IoT UEs, we design SPIN which

- solves the NTN UL synchronization problem by meeting the target accuracy requirements,
- utilizes both TDOA and FDOA measurements on PSS and SSS,
- includes tracking solutions to enable continuous positioning,
- achieves the theoretical bounds of position and velocity estimation accuracy,
- neither requires termination of the RRC connected mode nor interrupts the ongoing communication, thus resulting in minimal battery drain, and
- does not require any network modification additional reference signals, or extra control signaling.

SPIN firs estimates TOA and frequency of arrival (FOA) of SSs from one or more satellites. It then computes the differences between TOA and FOA measurements to get TDOA and FDOA measurements, respectively. Finally, SPIN estimates the UE's position and velocity from the joint set of TDOA and FDOA measurements, which it uses to compute and compensate residual TA and Doppler.

C. Contributions

We summarize the contributions of this paper as follows:

- We design a new positioning algorithm called SPIN, to specificall address the UL synchronization problem in NTN IoT UEs, and explain the key operations involved.
- We design SPIN by exploiting appropriate state-of-the-art signal processing techniques including fast Fourier transform (FFT), correlation, and fin resolution curve fitting and joint TDOA and FDOA based positioning, with an objective to achieve the theoretical bounds of position and velocity estimation accuracy.
- We provide comprehensive analyses that include discussion on theoretical bounds of position and velocity accuracy, i.e., Cramér-Rao lower bound (CRLB), and energy consumption of SPIN.
- We perform a thorough simulation based evaluation which includes physical layer (PHY) simulation to evaluate TOA and FOA estimations, and system level simulation to evaluate the fina positioning accuracy, and compare with CRLB. For the system level simulation, we consider an appropriate model which consists of a reference satellite constellation and global uniform distribution of UEs. We also perform comparison of battery life impact of SPIN with that of GNSS-based solution and the evaluation of the computational complexity associated with SPIN.

To the best of our knowledge, the positioning solution designed in this paper, which is particularly tailored for low-cost and low-power NTN IoT UEs, and solves the UL synchronization problem, is the firs of its kind.

Some of the notations and operations used in the paper are as follows.

- $*$ represents the convolution operation between two functions.
- $\langle \cdot, \cdot \rangle$ represents the vector dot product operation.
- $\|\cdot\|$ represents the vector magnitude.
- The bold face letters indicate vectors or matrices.
- The superscript $(\cdot)^*$ represents the complex conjugate operation.
- $|(\cdot)|$ denotes the magnitude operation.
- $\hat{(\cdot)}$ represents an estimated parameter.
- $\dot{(\cdot)}$ represents the time derivative of $(\cdot)$.
- The subscript $M \times N$ represents the size of the matrix in terms of its number of rows and columns.
- The superscripts $(\cdot)^T$ and $(\cdot)^{-1}$ denote matrix transpose and inverse operations, respectively.
- $\mathbf{0}_{M \times N}$ denotes a zero matrix of size $M \times N$.
- $[\boldsymbol{A}]_{ij}$ represents the element of matrix $\boldsymbol{A}$ located on the ith row and jth column.

Outline: The rest of the paper is organized as follows. We present the preliminaries including the system model and target requirements in Section II, and the SPIN algorithm in Section III. We discuss the theoretical bounds of positioning accuracy and the energy consumption in Section IV, and their numerical results and computational complexity in Section V. In Section VI, we briefl discuss the behavior of our positioning algorithm under additional scenarios. Finally, conclusions are drawn in Section VII.

II. Preliminaries

A. System Model

We consider an NTN which consists of one or more LEO satellites orbiting the earth, terrestrial UEs, gateway, radio access network (RAN) and core network (CN), as shown in Fig. 1. The NTN illustration shown in Fig. 1 depicts a transparent payload type architecture where the RAN is located on the earth [1], [2]. Conversely, there is regenerative payload type architecture where the RAN is located on-board the satellite [1], [2]. However, our design of SPIN is agnostic to the network architecture and hence works in both cases. In an NTN, the radio link which serves the UEs is referred to as the service link, whereas the one which connects the satellite with the gateway is called the feeder link. In the service link, the UEs are served by one or more beams from the satellite, where single or multiple beams can correspond to a cell depending on the network implementation [1]. When the NTN consists of a constellation of satellites, optionally,

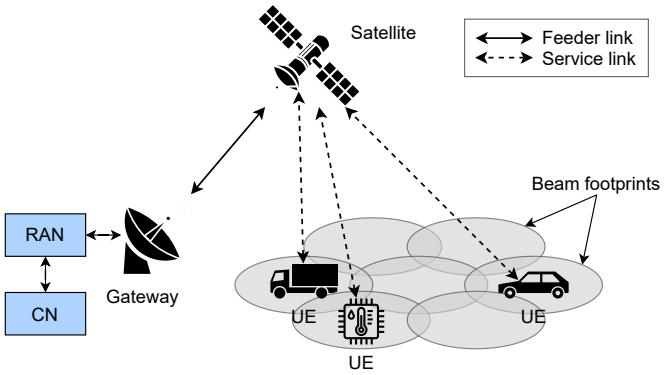

Fig. 1. An illustration of a non-terrestrial network.

inter-satellite links (ISL) exist between them. The backhaul consists of the RAN, e.g., 5G RAN, which enables the cellular communication through the selected radio access technology (RAT), and the CN, which connects eventually to the data network. To serve the NTN IoT applications, 3GPP has chosen NB-IoT and LTE-M, the standards which are already implemented and currently in use in the terrestrial cellular networks [18]. Using NB-IoT and LTE-M standards for NTN IoT applications gives several advantages. We can reuse the existing infrastructure, which minimizes implementation cost, and also gives stable and predictable performance. Therefore, in our work, we consider NB-IoT and LTE-M standards as the baseline RATs to design and evaluate our solution.

1) Radio Access Technology: As we discussed above, we design and evaluate SPIN by considering NB-IoT and LTE-M as the underlying RATs. While 3GPP considers Ka-band (20 GHz) frequency for NR NTN, which enables high data rate applications, it chooses S-band (2 GHz) for NTN-IoT, which is ideal for IoT applications. Both NB-IoT and LTE-M standards use orthogonal frequency division multiplexing (OFDM) modulated signals for communication. The NB-IoT and LTE-M OFDM signals are structured as 1 ms time units called subframes (SFs), which consist of 14 OFDM symbols. In the frequency domain, the OFDM subcarriers are usually spaced 15 kHz apart in both UL and DL for LTE-M and NB-IoT. Additionally, the BS can also configur the UL subcarrier spacing (SCS) in NB-IoT as 3.75 kHz. Further, physical random access channel (PRACH) has multiple options for SCS depending on the selected PRACH format. While the LTE-Category M1 (LTE-Cat M1) standard, the widely used LTE-M variant, occupies a bandwidth of 1.4 MHz, the NB-IoT standard uses a narrow bandwidth of 180 kHz. To enable synchronized communication between the BS and the UEs, LTE-M and NB-IoT standards periodically broadcast PSS, SSS and NPSS, NSSS, respectively. These SSs are implemented using standard sequences such as Zadoff-Chu (ZC) and/or m-sequences, which hold excellent correlation properties. In the following, unless the standard is specificall mentioned, we use the general terms SS, PSS, and SSS to indicate synchronization signals in both LTE-M and NB-IoT.

The PSS and SSS are known to the UE immediately after the DL sync. From the numerical values of CRLB discussed in Section IV, we observe that these SSs have sufficien bandwidth and duration to be utilized for positioning. Hence, we propose to use PSS, SSS and NPSS, NSSS in LTE-M and NB-IoT respectively, for the purpose of positioning in SPIN. The DL SSs received at the UE can be represented as

$$r_{\mathrm{s}}(t) = (s * h)(t) + w(t), \tag{1}$$

where s is the transmitted SS which includes both PSS and SSS, $w(t)$ are additive white Gaussian noise (AWGN) samples, which are assumed to be $w(t) \sim \mathcal{N}(0, \frac{N_0}{2})$, and h is the impulse response of the NTN channel. The latter is modelled by

$$h(t) = \sum_{i=1}^{L} \alpha_i(t) \exp(\mathrm{j}2\pi f_{\mathrm{o},i} t)\delta(t - \tau_{\mathrm{o},i}), \tag{2}$$

where L is the number of paths in the channel and α_i, $\tau_{\mathrm{o},i}$, and $f_{\mathrm{o},i}$ are the attenuation, time offset, and frequency offset of ith channel path, respectively. In addition to small scale fading which is caused mainly due to the UE velocity and the obstacles close to the UE, $\tau_{\mathrm{o},i}$ and $f_{\mathrm{o},i}$ also include time of fligh from the satellite to the UE and the Doppler shift due to satellite velocity, respectively [2]. It follows that, the signal $r_{\mathrm{s}}(t)$ is acquired by the UE at a sampling rate, $f_{\mathrm{s}} = 1/T_{\mathrm{s}}$, resulting in a discrete time signal, $r_{\mathrm{s}}(nT_{\mathrm{s}})$, where $n = 0, \pm1, \pm2, \ldots$ is the discrete time index. In the following, for simplicity, we use $r_{\mathrm{s}}(n)$ to represent $r_{\mathrm{s}}(nT_{\mathrm{s}})$.

2) Synchronization Process: During DL synchronization, an IoT UE performs a series of operations on the received DL signal to get time and frequency synchronization [27]. In an NTN, the DL SSs are already pre-compensated at the BS for the common Doppler with respect to an RP in the cell. Therefore, the received frequency, f_{RX}, suffers only from the residual component of Doppler depending on the displacement of the UE from the RP. We show an illustration of the synchronization process and the associated frequency errors in Fig. 2. The UE and BS oscillator errors are represented by x_1 and x_2 parts per million (ppm), respectively. On the other hand, the offset between the DL transmit (TX) and receive (RX) frequencies, which results from the residual Doppler, is denoted by x_3 ppm. In Fig. 2, we see that the frequency offset estimated by the UE in DL synchronization is the sum of the residual Doppler and the oscillator errors. Subsequently, the UE adjusts its frequency to f_{RX} and transmits UL signal at a frequency spaced at duplex distance away from f_{RX}. On the received signal, the satellite performs post-compensation of the common Doppler offset with respect to the RP to partially compensate for the Doppler effect in UL channel. The resultant signal experiences a frequency offset of twice the residual Doppler offset as shown in Fig. 2. The values of residual frequency offsets for different LEO orbits and beam configuration denoted by sets 1-4[2] are given in Table I [11], [28]. It should be noted that the maximum allowed frequency offset in UL as per the standard is 0.1 ppm [29]. However, from Table I, it is evident that the residual frequency offsets in NTN are significantl high compared to the allowed limit.

[2]The beam configuratio sets given in Table I refer to the satellite sets define in [1], [18], which differ in terms of antenna parameters and the resulting beams.

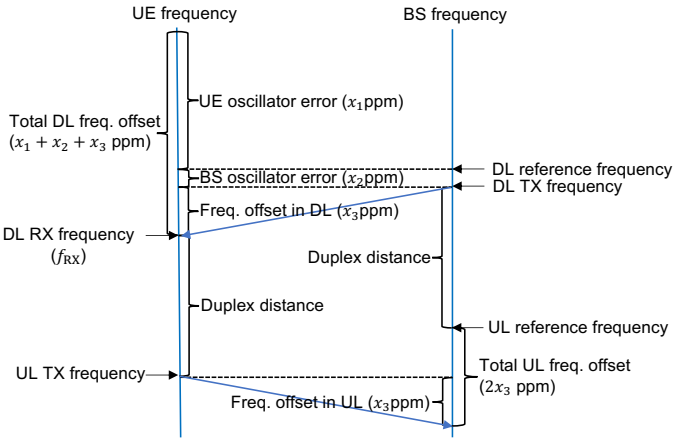

Fig. 2. UL synchronization in NTN [11].

TABLE I
UL RESIDUAL FREQUENCY OFFSET IN PPM

Beam configuration	LEO 1200 km	LEO 600 km
Set 1	1.92	2.20
Set 2	3.92	3.86
Set 3	21.56	21.14
Set 4	-	39.90

In addition to the above method of UL synchronization, [11] discusses another option where the UE pre-compensates its UL signal by the total frequency offset estimated in the DL. For the sake of conciseness, we do not explain that option here. It could be noted that, for sets 1 and 2, the alternative method results in higher residual frequency offsets than the method discussed above. However, for the other beam configuration sets, it provides residual frequency offsets similar to or better than that of the method discussed above. Nevertheless, both the synchronization options are inadequate as they result in residual frequency offsets higher than 0.1 ppm, which is the limit set by the standard. Similarly, after the DL synchronization process, the UE time synchronization also suffers from residual TA with respect to the RP in the cell. For all the reasons discussed above, the options currently available for UL synchronization in NTN are insufficient.

3) Reference Coordinate System and Satellite Constellation: For SPIN, we consider the earth-centered earth-fixed (ECEF) coordinate system, which is a Cartesian coordinate system where the axes are named as X, Y, and Z in three-dimensional space [15, Ch. 2]. The ECEF system is termed earth-centered since the origin is the center of mass of the earth, i.e., the *geocenter*, and earth-fixed since the coordinate system is fixed with respect to the earth, i.e., the axes rotate along with the earth. The Z-axis aligns with the rotation axis of the earth and hence passes through the geocenter and the north pole. Furthermore, the X-axis intersects the equator of the earth at the *Greenwich meridian*. Finally, the Y axis is defined with reference to the X-axis such that it completes a right-handed orthogonal coordinate system. Compared to other coordinate systems, ECEF system is more convenient to calculate the line-of-sight (LOS) distance between two

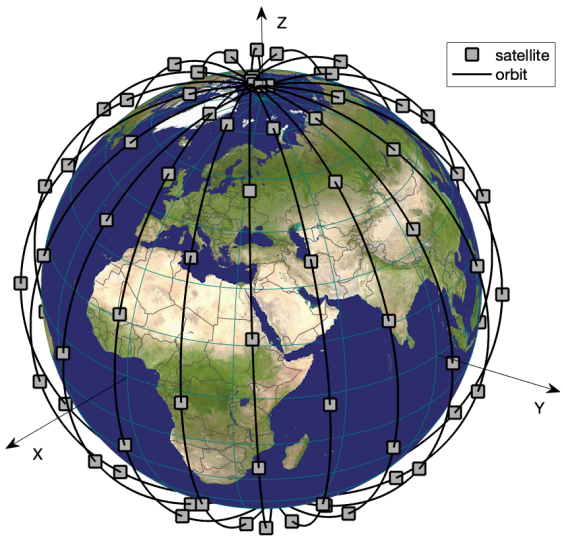

Fig. 3. An illustration of LEO satellite constellation around the earth, represented in an ECEF coordinate system. The earth is plotted using [33].

points [15, Ch. 2]. Therefore, it is ideal for SPIN that considers TDOA measurements which are functions of pseudo-range difference measurements. Moreover, global positioning system (GPS), the widely used GNSS solution which is owned and operated by the USA, adopts ECEF for positioning. This also makes ECEF a preferable coordinate system for SPIN, which effectively operates as an alternative to GNSS.

For the design and evaluation of SPIN, we consider a reference constellation which is represented in the standard format, $i : t/p/f$, where i is the inclination of the orbital plane, t is the total number of satellites, p is the number of orbital planes, and f is the phasing parameter which denotes the relative spacing between the adjacent orbital planes [30], [31]. In our evaluation, we consider a near-polar Walker-star LEO satellite constellation, which gives global coverage with simple constellation design [32]. Regardless, SPIN is agnostic to the type of constellation and works if the UE gets visibility to a sufficient number of satellites. In Fig. 3, we show an example of a LEO near-polar Walker star constellation which uses a pattern of $87.5° : 100/10/5$, represented in an ECEF coordinate system.

In the design and evaluation of SPIN, we use the following notations to represent the position and velocity vector in the ECEF coordinate system. Let $[x_i\ y_i\ z_i]$ and $[v_{x_i} v_{y_i} v_{z_i}]$ be the position coordinates and the velocity vector of the satellite, respectively. Since SPIN uses a set of multiple measurements from the satellites, which we define in later sections, the subscript i denotes the index of the associated measurement in the set. Further, we represent the unknown location coordinates and the velocity vector of the UE as $\boldsymbol{X} = [x\ y\ z]$ and $\boldsymbol{V} = [v_x\ v_y\ v_z]$, respectively.

B. Target Requirements

In the following, we find the upper bound of the positioning error for solving the UL synchronization issues. To begin with,

the Doppler shift, f_{Doppler}, experienced in an NTN relative to the carrier frequency, f_{c}, is given by

$$\frac{f_{\text{Doppler}}}{f_{\text{c}}} = \frac{\langle \boldsymbol{V}_{\text{sat-UE}}, \boldsymbol{U}_{\text{sat-UE}} \rangle}{c \left\| \boldsymbol{U}_{\text{sat-UE}} \right\|}, \tag{3}$$

where $\boldsymbol{V}_{\text{sat-UE}}$ is the relative velocity between the satellite and the UE, $\boldsymbol{U}_{\text{sat-UE}}$ is the position vector from the satellite to the UE, and c is the speed of light. The firs order Doppler error [34] is given by

$$F_{\text{e}} = \frac{\Delta f_{\text{Doppler}}}{f_{\text{c}}} = \underbrace{\langle \boldsymbol{V}_{\text{sat-UE}}, \boldsymbol{P}_{\boldsymbol{U}_{\text{sat-UE}}} \frac{\Delta \boldsymbol{U}_{\text{sat-UE}}}{c \left\| \boldsymbol{U}_{\text{sat-UE}} \right\|} \rangle}_{P_{\text{e}}} + \underbrace{\langle \Delta \boldsymbol{V}_{\text{sat-UE}}, \frac{\boldsymbol{U}_{\text{sat-UE}}}{c \left\| \boldsymbol{U}_{\text{sat-UE}} \right\|} \rangle}_{V_{\text{e}}}, \tag{4}$$

where $\Delta f_{\text{Doppler}}$ is the Doppler error, $\Delta \boldsymbol{V}_{\text{sat-UE}}$ is the relative velocity error, $\Delta \boldsymbol{U}_{\text{sat-UE}}$ is the error in position vector $\boldsymbol{U}_{\text{sat-UE}}$, and $\boldsymbol{P}_{\boldsymbol{U}_{\text{sat-UE}}}$ is the orthogonal projection to $\boldsymbol{U}_{\text{sat-UE}}$. Hence, P_{e} is the portion of the Doppler error attributed to position error, and V_{e} is the portion attributed to relative velocity error. From (4), the position and relative velocity errors can be expressed as

$$\left\| \Delta \boldsymbol{U}_{\text{sat-UE}} \right\| \leq P_{\text{e,max}} \frac{c}{\boldsymbol{V}_{\text{sat-UE}}} \left\| \boldsymbol{U}_{\text{sat-UE}} \right\| \tag{5}$$

and

$$\left\| \Delta \boldsymbol{V}_{\text{sat-UE}} \right\| \leq V_{\text{e,max}} c, \tag{6}$$

respectively. In (5) and (6), $P_{\text{e,max}}$ and $V_{\text{e,max}}$ represent the portion of the maximum Doppler error attributed to error in position and velocity respectively, and they are related to the maximum Doppler error, $F_{\text{e,max}}$, as,

$$F_{\text{e,max}} = P_{\text{e,max}} + V_{\text{e,max}}. \tag{7}$$

The achievable satellite position and velocity accuracy available in the public domain [35] are

$$\left\| \Delta \boldsymbol{U}_{\text{sat}} \right\| \leq 3 \text{ m} \tag{8}$$

and

$$\left\| \Delta \boldsymbol{V}_{\text{sat}} \right\| \leq 0.2 \text{ m/s}. \tag{9}$$

As per 3GPP standards, a maximum frequency error of 0.1 ppm is allowed in the UL to facilitate successful reception at the BS [29]. Since the Doppler shift due to UE velocity in NTN is same as that of a terrestrial network [11], we disregard the UE velocity factor in the following. Hence, we replace $\Delta \boldsymbol{V}_{\text{sat-UE}}$ with $\Delta \boldsymbol{V}_{\text{sat}}$, and we compute $V_{\text{e,max}}$ from (6) using (9). In the NR UL synchronization study conducted in [34], 80% of the frequency error is attributed to the local oscillator drift after DL synchronization and the remaining 20% to the residual Doppler shift. Since the residual Doppler error in the UL is twice the one-sided Doppler, the maximum Doppler pre-compensation error, $F_{\text{e,max}}$, is 0.01 ppm for the above error ratio. Now, we consider LEO satellite at an altitude of 600 km and a velocity of 7.69 km/s. We approximate $\left\| \boldsymbol{U}_{\text{sat-UE}} \right\|$ by the satellite orbit altitude, which is the minimum distance between the UE and the satellite. Using the above error ratio, $V_{\text{e,max}}$, (5), and (7), we compute the allowed position error, $\left\| \Delta \boldsymbol{U}_{\text{sat-UE}} \right\|_{\text{max}} = 218.5$ m. To guarantee the overall positioning error requirement represented by $\left\| \Delta \boldsymbol{U}_{\text{sat-UE}} \right\|_{\text{max}}$, the satellite and UE position error should satisfy

$$\left\| \Delta \boldsymbol{U}_{\text{UE}} \right\| + \left\| \Delta \boldsymbol{U}_{\text{sat}} \right\| \leq \left\| \Delta \boldsymbol{U}_{\text{sat-UE}} \right\|_{\text{max}}. \tag{10}$$

Considering the worst-case satellite position error, represented by $\left\| \Delta \boldsymbol{U}_{\text{sat}} \right\|_{\text{max}}$, the UE position error should satisfy

$$\begin{aligned} \left\| \Delta \boldsymbol{U}_{\text{UE}} \right\| &\leq \left\| \Delta \boldsymbol{U}_{\text{sat-UE}} \right\|_{\text{max}} - \left\| \Delta \boldsymbol{U}_{\text{sat}} \right\|_{\text{max}} \\ &= 218.5 - 3 = 215.5 \text{ m}. \end{aligned} \tag{11}$$

If the above limit is satisfie by UE positioning, the overall positioning error requirement is guaranteed, provided the satellite position error does not exceed 3 m.

We performed the above analysis for a fi ed error budget of $80\% - 20\%$ between local oscillator offset and Doppler shift errors. However, in practice, the oscillator errors in the UE can be different. Therefore, we have also plotted the allowed position errors for different error budget allocations in Fig. 4. In the figure we show the allowed maximum UE position error for different values of possible local oscillator error. The local oscillator error is represented in terms of percentage of the maximum frequency error in the UL allowed by the standard. For example, when the local oscillator error is 80% of the maximum uplink frequency error, i.e., 0.1 ppm, the tolerance in UE positioning error is 20%, which corresponds to 215.5 m.

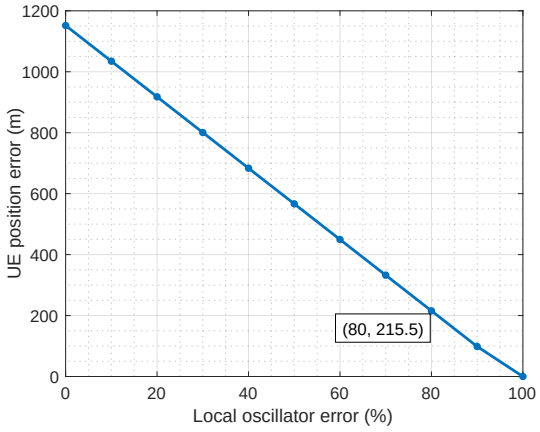

Fig. 4. Maximum allowed position error for varying local oscillator error.

In the above, we discussed about the UL frequency synchronization problem and the target requirement for UE positioning to resolve the issue. As we already discussed in Section I, UL time synchronization also faces issues. For successful detection at the BS, the timing error should be within $\pm \frac{\text{CP}}{2}$, where CP is the cyclic prefix Correspondingly, the required positioning accuracy is given by $\left\| \Delta \boldsymbol{U}_{\text{sat-UE}} \right\| \leq \frac{\text{CP}}{4} c = \pm 7250$ m [34]. Compared to the UL frequency synchronization problem, residual TA problem requires more relaxed positioning accuracy. Therefore, we consider the accuracy needed for UL frequency sync as the target requirement for our positioning solution.

III. SPIN

We design SPIN by utilizing the varying TOA and FOA of the DL SSs transmitted by one or more satellites. We

TABLE II
SUMMARY OF FEATURES IN PRIOR-ART POSITIONING SOLUTIONS COMPARED WITH SPIN.

Features \ Solutions	[7]	[42]	[24]	[43]	[17]	[39]	[44, Ch. 5]	[41]	SPIN
NTN	✓	✓	×	×	×	×	✓	×	✓
IoT	×	×	✓	×	×	×	×	×	✓
PSS	✓	×	×	✓	×	×	×	×	✓
SSS	×	×	×	✓	×	×	×	×	✓
Fine resolution/ curve fittin	×	×	×	×	×	×	×	×	✓
TDOA	✓	✓	✓	✓	✓	✓	✓	✓	✓
FDOA	×	✓	×	×	✓	×	✓	×	✓
Taylor series/ iterative	✓	✓	✓	×	×	✓	✓	✓	✓
Weighted iterative	×	✓	✓	×	×	✓	×	✓	✓
2-WLS/ 2-WLS initialize	×	×	×	×	✓	×	✓	✓	✓
Time multiplexed tracking	×	×	×	×	×	×	×	×	✓
Self positioning	✓	✓	×	✓	✓	-	✓	✓	✓
Solves UL sync problem	*	*	×	*	*	*	*	*	✓

* represents that the solution has either insufficien accuracy or the accuracy has not been evaluated.

consider SSs that are transmitted by either a single satellite at different instants of time or multiple satellites at same or different instants of time on different frequency carriers. Since TOA and FOA measurements suffer from UE clock time and frequency offsets, they are error-prone to be directly used for positioning. Therefore, SPIN takes differences between TOA and FOA measurements to obtain TDOA and FDOA measurements, respectively. Next, we need to solve UE position and velocity from the TDOA and FDOA measurements, which is a nonlinear and non-convex problem [36]. There are several state-of-the-art solutions available which can be broadly classifie into two categories. The firs category consists of two-step weighted least squares (2-WLS) solutions, which give closed-form position and velocity estimates [17], [37]. 2-WLS methods represent the nonlinear equations in linear form by adding additional unknown nuisance parameters. 2-WLS and modifie 2-WLS methods discussed in the literature have very low computational complexity [17], [37]. However, these methods suffer from poor accuracy due to high bias [38]. In the second category of methods, position and velocity are obtained using iterative algorithms [39], [40]. Unfortunately, unless sufficientl accurate initial position and velocity are assumed, these methods converge to wrong local minima, resulting in high error. Foy's method, alternatively called Taylor series-based weighted least squares (TWLS) method, is one such iterative method [39]. TWLS uses the firs order Taylor series to approximate the nonlinear equations as linear and solves them iteratively using weighted least squares. In [41], 2-WLS method is used to obtain rough estimate of position which then initializes the TWLS method. Finally, TWLS method delivers fin position estimates. Inspired from [41], we adopt a similar method for SPIN in the context of IoT NTN. We use the 2-WLS method to get rough estimates of position and velocity and use them to initialize TWLS, which finall delivers fine estimates.

Like any other real-time positioning solutions, SPIN incorporates an acquisition block which acquires position for the firs time during a cold-start. A UE usually performs acquisition when it is in RRC idle mode and gets a UL data request from the upper layers. Before initiating the connection request, the UE requires its own position to compute and compensate the residual Doppler during RA. In this case, the UE does not have valid measurements from the past to be used for positioning. However, after obtaining position and velocity fi by acquisition, SPIN maintains the accuracy within acceptable limits by performing tracking. SPIN performs this tracking operation in a time-multiplexed manner with the ongoing NTN cellular communication, which makes it unique from the prior-art solutions. We provide a summary of the features supported in relevant prior-art positioning solutions and our solution in Table II. In the following, we defin SPIN by firs introducing the SPIN block diagram, and then having a detailed discussion of the individual blocks and the operations involved in the positioning algorithm.

We show the block diagram of SPIN in Fig. 5, which mainly consists of three blocks, namely, TDOA and FDOA estimation, SPIN acquisition, and SPIN tracking. In the following, we explain each of these blocks and their functions.

A. TDOA and FDOA Estimation

1) TOA and FOA Estimation: SPIN firs performs TOA and FOA measurements on SSs arriving from one or more satellites over a period called SPIN window (W_{SPIN}). For TOA and FOA estimation, SPIN reuses a part of the synchronization algorithm used in cellular DL and performs some additional operations. For instance, when SPIN operates in an NB-IoT UE, it can reuse the cellular NB-IoT DL synchronization algorithm to get time and frequency synchronization. An example of a low-complexity synchronization method for NB-IoT is given in [27]. If the NB-IoT UE uses this method, SPIN can reuse the sliding auto-correlation based synchronization detection and coarse time-frequency synchronization as dis-

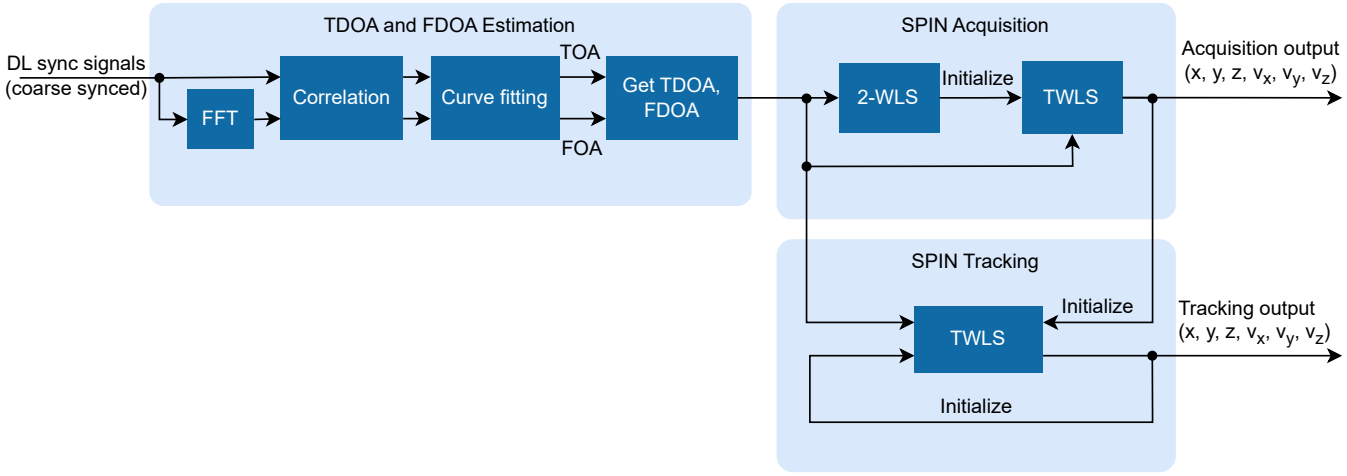

Fig. 5. Block diagram of SPIN.

cussed in [27]. The coarse synchronization is followed by a fin synchronization step which involves cross-correlation of the received signal with the known templates of PSS. Since the channel SNR may vary depending on the coverage scenario, the correlation may require several synchronization signals to be combined. The UE may perform 1 ms coherent combining [45] followed by incoherent combining over longer duration to synchronize successfully. A successful synchronization detection delivers TOA and FOA estimates. However, the accuracy of these estimates are insufficien for SPIN mainly for two reasons. First, the cellular synchronization process in the UE does not necessarily use SSS to obtain the synchronization, especially during the initial cell access when the SSS sequence is unknown to the UE. Second, the TOA and FOA accuracies are largely affected by the finit sampling rate. Regardless, SPIN utilizes the time and frequency synchronization output of the DL synchronization process to refin the time-frequency search space. However, to achieve the target positioning accuracy, SPIN performs some additional operations.

First, SPIN performs cross-correlation of combined PSS and SSS templates with the received signal. Like the frequency offset estimation in cellular UEs [46], SPIN estimates FOA by frequency-domain cross-correlation. To this end, the correlation block in Fig. 5 performs two types of cross-correlations, pre-FFT cross-correlation to estimate TOA and post-FFT cross-correlation to obtain FOA. The pre- and post-FFT signal correlations are represented by

$$\rho(\tau) = \sum_{n} r_{\mathrm{s}}(n) s^{*}(n+\tau) \tag{12}$$

and

$$\Lambda(\varphi) = \sum_{k} R_{\mathrm{s}}(k) S^{*}(k+\varphi), \tag{13}$$

respectively, where $s(n)$ is the SS template in discrete form sampled at f_{s}, $R_{\mathrm{s}}(k)$ and $S(k)$ are the FFTs of $r_{\mathrm{s}}(n)$ and $s(n)$, respectively. τ and φ are the pre- and post-FFT cross correlation lags, respectively. The lags at which the cross-correlation peaks occur in (12) and (13) are found by

$$\hat{\tau} = \arg\max_{\tau} |\rho(\tau)| \tag{14}$$

and

$$\hat{\varphi} = \arg\max_{\varphi} |\Lambda(\varphi)|, \tag{15}$$

respectively.

Second, SPIN incorporates fine-resolutio curve fitting which operates on the magnitude of pre- and post-FFT cross correlation outputs to get fine TOA and FOA estimates. To this end, we use 3-point parabolic curve fittin [47] which uses the peak value of the cross-correlation magnitude and its adjacent two values. The fractional offsets from the estimated peak to the fine-resolutio peak obtained using 3-point parabolic curve fittin on pre- and post-FFT correlation outputs are given by

$$\delta_{\tau} = \frac{|\rho(\hat{\tau}-1)| - |\rho(\hat{\tau}+1)|}{2\big(|\rho(\hat{\tau}-1)| - |\rho(\hat{\tau})| + |\rho(\hat{\tau}+1)|\big)} \tag{16}$$

and

$$\delta_{\varphi} = \frac{|\Lambda(\hat{\varphi}-1)| - |\Lambda(\hat{\varphi}+1)|}{2\big(|\Lambda(\hat{\varphi}-1)| - |\Lambda(\hat{\varphi})| + |\Lambda(\hat{\varphi}+1)|\big)}, \tag{17}$$

respectively. Note that curve-fittin based fin estimators are biased estimators [47]. However, from our evaluations, we observe that the bias in our case is negligible and hence the performance is not affected. The resulting TOA and FOA estimates achieve the CRLB, which is the theoretical bound for an unbiased estimator.

It should be noted that the FOA estimated using the above steps do not include the common Doppler shift with respect to the RP in the cell. This is due to the Doppler pre-compensation already performed by the BS on the DL SSs. Since the FOA measurements are possibly acquired from multiple satellites, the common Doppler may be different for different FOA measurements. Therefore, to get correct positioning, satellite-specifi common Doppler needs to be added back to get the actual FOA estimates. For this purpose, SPIN computes the

common Doppler, which can be easily done using the satellite ephemeris and the coordinates of the RP.

The fin resolution TOA and FOA estimates obtained after curve fittin are given by

$$t_{\mathrm{TOA},i} = \frac{1}{f_{\mathrm{s}}}(\hat{\tau}_i + \delta_{\tau,i}), \qquad i = 1, 2, \ldots, N, \tag{18}$$

and

$$f_{\mathrm{FOA},i} = \frac{f_{\mathrm{s}}}{N_{\mathrm{FFT}}}\,(\hat{\varphi}_i + \delta_{\varphi,i}) + f_{\mathrm{com},i}, \qquad i = 1, 2, \ldots, N, \tag{19}$$

respectively, where the subscript i denotes the measurement index, N is the total number of measurements, N_{FFT} is the length of the FFT, and $f_{\mathrm{com},i}$ is the common Doppler with respect to the RP. Now, we compute range measurements, r_i, using the fin TOA measurements, $t_{\mathrm{TOA},i}$, as

$$r_i = c \cdot t_{\mathrm{TOA},i}, \qquad i = 1, 2, \ldots, N. \tag{20}$$

Similarly, we compute range rate [42], $\dot{r}_i$, using fin resolution FOA measurements, $f_{\mathrm{FOA},i}$, as

$$\dot{r}_i = -\frac{c}{f_{\mathrm{c}}} f_{\mathrm{FOA},i}, \qquad i = 1, 2, \ldots, N. \tag{21}$$

Next, we relate these range measurements and the UE and satellite position and velocity vectors by (22), where ΔT is the interval between consecutive TOA/FOA measurements, η_{TO} is the effective time offset due to satellite and UE clock deviations, and n_i is the estimation error in the ith range measurement which conforms to the Gaussian distribution $\mathcal{N}(0, \sigma^2_{n_i})$. Similarly, the range rate measurements can be expressed as (23), where η_{FO} is the effective frequency offset due to satellite and UE local oscillator offsets, and n'_i is the estimation error in the ith range rate measurement which conforms to the Gaussian distribution $\mathcal{N}(0, \sigma^2_{n'_i})$. It should be noted that the mathematical model define above is applicable to both acquisition and tracking and hence ΔT could be replaced by either acquisition interval or tracking interval, which are define later in this section.

In the next step, to eliminate the UE clock and local oscillator offsets in (22) and (23), we take differences between TOA and FOA estimates to get TDOA and FDOA measurements, respectively.

2) TDOA and FDOA Measurements: For N TOA estimates, there are $\frac{N(N-1)}{2}$ possible TDOA measurements. However, when the received signal is cross-correlated with the clean template of SSs, only $N-1$ TDOAs are sufficient This is due to the fact that the remaining combinations result in redundant TDOA adding no extra information [48]. $N-1$ TDOAs can be generated either by taking the difference with respect to a single arbitrary reference TOA or by taking differences between the adjacent TOA measurements, which we refer to as adjacent TDOA [7]. Adjacent TDOA is particularly useful in continuous SPIN tracking which comprises of a sliding time window which includes new TOA measurements while dropping old measurements continuously over time. When adjacent TDOA is used in a continuous tracking scenario, a fi ed number of stale TDOA get dropped when the same number of fresh TDOA get added, whereas the rest of the TDOA measurements remain unchanged between the tracking loops. The above reasoning is also applicable for getting FDOA values from the FOA measurements. Without loss of generality, we assume adjacent TDOA and FDOA in the following. Thus, we get range and range rate difference measurements, which are the scaled versions of TDOA and FDOA, as

$$r_{ij} = r_i - r_j = c(t_{\mathrm{TOA},i} - t_{\mathrm{TOA},j}) \tag{24}$$

and

$$\dot{r}_{ij} = \dot{r}_i - \dot{r}_j = -\frac{c}{f_{\mathrm{c}}}(f_{\mathrm{FOA},i} - f_{\mathrm{FOA},j}), \tag{25}$$

respectively, where $i = 2, 3, \ldots, N$ and $j = i-1$. Substituting (24) and (25) into (22) and (23), respectively, we obtain

$$r_{ij} = f_i(\boldsymbol{X}, \boldsymbol{V}) - f_j(\boldsymbol{X}, \boldsymbol{V}) + \xi_{ij} \tag{26}$$

and

$$\dot{r}_{ij} = g_i(\boldsymbol{X}, \boldsymbol{V}) - g_j(\boldsymbol{X}, \boldsymbol{V}) + \xi'_{ij}, \tag{27}$$

where $i = 2, 3, \ldots, N$, $j = i-1$, $\xi_{ij} = n_i - n_j$, $\xi'_{ij} = n'_i - n'_j$ and $f_i(\cdot)$ and $g_i(\cdot)$ are the functions indicated in (22) and (23), respectively. We denote the set of $2(N-1)$ range and range rate difference measurements obtained in this step as

$$\boldsymbol{\phi} = [r_{21}, r_{32}, \ldots, r_{N\ N-1}, \dot{r}_{21}, \dot{r}_{32}, \ldots, \dot{r}_{N\ N-1}]^{\mathrm{T}}. \tag{28}$$

In the next step, we use (26) and (27) to estimate the UE position and velocity.

B. SPIN Acquisition

When a position fi is required before initiating an RRC connection, SPIN performs UE location acquisition. SPIN acquisition involves obtaining TDOA and FDOA measurements from the SSs over a time window called SPIN acquisition window ($W_{\mathrm{SPIN,acq}}$). We call the time duration of incoherent

$$r_i = \underbrace{\sqrt{\big(x_i - (x + v_x i\Delta T)\big)^2 + \big(y_i - (y + v_y i\Delta T)\big)^2 + \big(z_i - (z + v_z i\Delta T)\big)^2}}_{f_i(\boldsymbol{X}, \boldsymbol{V})} + c \cdot \eta_{\mathrm{TO}} + n_i, \qquad i = 1, 2, \ldots, N. \tag{22}$$

$$\dot{r}_i = \underbrace{\frac{(v_{x_i} - v_x)\big(x_i - (x + v_x i\Delta T)\big) + (v_{y_i} - v_y)\big(y_i - (y + v_y i\Delta T)\big) + (v_{z_i} - v_z)\big(z_i - (z + v_z i\Delta T)\big)}{\sqrt{\big(x_i - (x + v_x i\Delta T)\big)^2 + \big(y_i - (y + v_y i\Delta T)\big)^2 + \big(z_i - (z + v_z i\Delta T)\big)^2}}}_{g_i(\boldsymbol{X}, \boldsymbol{V})} + \frac{c}{f_{\mathrm{c}}}\eta_{\mathrm{FO}} + n'_i,$$

$$i = 1, 2, \ldots, N. \tag{23}$$

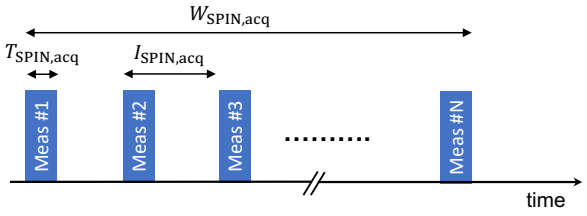

Fig. 6. Timing diagram of SPIN acquisition.

combining required for each TOA/FOA measurement as SPIN acquisition duration ($T_{\text{SPIN,acq}}$). We decide $T_{\text{SPIN,acq}}$ based on the duration needed for successful synchronization for the maximum coupling loss (MCL) under consideration [18], [27]. The interval between successive TOA/FOA measurements in the acquisition is referred to as SPIN acquisition interval ($I_{\text{SPIN,acq}}$). We show the SPIN acquisition timing diagram in Fig. 6.

To perform positioning, in addition to TDOA and FDOA measurements, UE also requires the satellite position and velocity when the SSs were transmitted. As we mentioned in Section I, the network broadcasts satellite ephemeris in NTN system information broadcast (SIB). The UE can extrapolate the ephemeris acquired at the beginning of an RRC connection until the expiry of a network define timer called ephemeris validity timer [49].

From (26) and (27), we get a joint set of $2(N-1)$ nonlinear range and range rate difference equations, which are based on the TDOA and FDOA measurements taken during $W_{\text{SPIN,acq}}$. To begin with, SPIN uses the 2-WLS method to obtain initial rough estimates of UE position and velocity. In the firs step of 2-WLS, the non-linear equations are represented in linear form by adding two extra estimation parameters. Thus, including the UE position and velocity vectors, 8 parameters are estimated using WLS. In the second step, using the relation between the extra parameters and the UE position and velocity, the estimation is refine to the original 6 parameters. To avoid repetition, we do not provide the details of 2-WLS method here but refer to [17].

Next, SPIN performs TWLS to get fine estimates of UE position and velocity. In TWLS, the $2(N-1)$ nonlinear equations given by (26) and (27) are firs linearized using the first-orde Taylor series based linear approximation. The resulting equations can be expressed in the form

$$\boldsymbol{B} = \boldsymbol{A}\boldsymbol{\theta} + \boldsymbol{n}, \tag{29}$$

where $\boldsymbol{\theta} = [\boldsymbol{X}\ \boldsymbol{V}]^{\mathrm{T}}$ and $\boldsymbol{n} = [\xi_{21}, \xi_{32}, .., \xi'_{21}, .., \xi'_{N\ N-1}]^{\mathrm{T}}$. The WLS solution of (29) is given by

$$\hat{\boldsymbol{\theta}} = (\boldsymbol{A}^{\mathrm{T}}\boldsymbol{W}\boldsymbol{A})^{-1}\boldsymbol{A}^{\mathrm{T}}\boldsymbol{W}\boldsymbol{B}, \tag{30}$$

where $\boldsymbol{W}$ is a weight matrix of size $2(N-1)\times 2(N-1)$. The details of the Taylor series approximation and the definition of $\boldsymbol{A}$, $\boldsymbol{B}$, and $\boldsymbol{W}$ are given in the Appendix. The matrices $\boldsymbol{A}$ and $\boldsymbol{B}$ contain elements which are functions of initial values of the estimation parameters. The matrix $\boldsymbol{W}$ is also unknown initially and hence we firs compute that using the initial values of position and velocity. To get accurate estimates, further we perform several iterations of TWLS, every time updating $\boldsymbol{A}$, $\boldsymbol{B}$, and $\boldsymbol{W}$ using the position and velocity estimates obtained in the previous iteration.

The SPIN acquisition is summarized in Algorithm 1. In the algorithm, for all the parameters and matrices which are updated iteratively, we have added superscripts inside parentheses to indicate the iteration number. Since the weight for 2-WLS is unknown initially, we use the identity matrix to get an initial position fix. Then we compute the weight matrix for the 2-WLS using the estimated UE location and velocity. We perform 2-WLS again to get more accurate estimates. We run three iterations of such reweighted 2-WLS which are sufficien to eliminate the effect of the uninformed initial estimate [50]. Then we compute the weight matrix for TWLS using the UE location and velocity estimated from 2-WLS. We also use the 2-WLS estimation results to initialize the TWLS algorithm. We run TWLS iteratively until the convergence criterion is met, i.e., the difference in estimation results between successive iterations is confine below a sufficientl low threshold, ϵ_{th}. To accommodate for the 2-WLS and TWLS computations associated with SPIN, we include an extra processing time, $T_{\text{SPIN,proc}}$, after completing the measurements in the acquisition window. One can vary the value of $T_{\text{SPIN,proc}}$ to adjust the SPIN computational complexity based on the capability of the UE.

Algorithm 1: SPIN acquisition algorithm.

Input:
Range, range rate measurements: $\boldsymbol{\phi}$
Satellite positions: x_i y_i, z_i
Satellite velocities: v_{x_i}, v_{y_i}, v_{z_i}
Convergence threshold: ϵ_{th}
Maximum iteration: $k_{\max}$

Output:
UE position estimate: $\boldsymbol{X}^{(k)} = [x^{(k)}, y^{(k)}, z^{(k)}]$
UE velocity estimate: $\boldsymbol{V}^{(k)} = [v_x{}^{(k)}, v_y{}^{(k)}, v_z{}^{(k)}]$

Initialization: 2-WLS on $\boldsymbol{\phi}$
Initialize weight to $\boldsymbol{I}_{2(N-1)\times 2(N-1)}$;
$k = 0$;
while $k \leq 3$ **do**
  Estimate $\boldsymbol{X}^{(k)}, \boldsymbol{V}^{(k)}$ using 2-WLS;
  Update weight using $\boldsymbol{X}^{(k)}, \boldsymbol{V}^{(k)}$;
  $k = k + 1$;

TWLS Positioning: TWLS on $\boldsymbol{\phi}$
Compute $\boldsymbol{W}^{(0)}$, $\boldsymbol{A}^{(0)}$, $\boldsymbol{B}^{(0)}$ using $\boldsymbol{X}^{(k-1)}, \boldsymbol{V}^{(k-1)}$;
TWLS initialize: $\boldsymbol{X}_0 = \boldsymbol{X}^{(k-1)}$, $\boldsymbol{V}_0 = \boldsymbol{V}^{(k-1)}$;
$k = 0$;
Iteration error, $\epsilon^{(k)} = \infty$;
while $\epsilon^{(k)} \geq \epsilon_{\text{th}}$ *and* $k \leq k_{\max}$ **do**
  Estimate $\boldsymbol{X}^{(k)}, \boldsymbol{V}^{(k)}$ using TWLS;
  Compute $\boldsymbol{W}^{(k+1)}$, $\boldsymbol{A}^{(k+1)}$, $\boldsymbol{B}^{(k+1)}$ using $\boldsymbol{X}^{(k)}, \boldsymbol{V}^{(k)}$;
  TWLS initialize: $\boldsymbol{X}_0 = \boldsymbol{X}^{(k)}$, $\boldsymbol{V}_0 = \boldsymbol{V}^{(k)}$;
  $k = k + 1$;
  Compute iteration error $\epsilon^{(k)}$;

C. SPIN Tracking

After acquisition, SPIN performs tracking to maintain the position accuracy within acceptable limits. SPIN tracking uses a similar technique for positioning as in acquisition except for a few differences. SPIN tracking first initializes its TWLS using the UE location fix obtained by acquisition, and then tracks the location in loops by further initializing the TWLS using the position fixes obtained in the previous tracking loops. Like SPIN acquisition, tracking also involves a window called SPIN tracking window ($W_{\text{SPIN,track}}$), during which SPIN performs one full loop of tracking. During each $W_{\text{SPIN,track}}$, SPIN measures TOA and FOA by combining SSs for a duration of SPIN tracking duration ($T_{\text{SPIN,track}}$). The tracking measurements are done at an interval called SPIN tracking interval ($I_{\text{SPIN,track}}$). We show the SPIN tracking timing diagram in Fig. 7(a). Like SPIN acquisition, tracking also includes extra processing time, $T_{\text{SPIN,proc}}$, after the tracking window.

Unlike SPIN acquisition which is usually performed before initiating an RRC connection, SPIN tracking does not get abundant time gaps. Therefore, we propose two methods for SPIN tracking based on the availability of time gaps for positioning.

1) Periodic SPIN Tracking: Periodic SPIN tracking involves tracking periodically at fixed intervals which provides the UE with high positioning accuracy that remains valid for a long time. To this end, we define a timer called SPIN position validity timer, $T_{\text{SPIN,val}}$, upon the expiry of which SPIN periodic tracking is mandatory. Thus, periodic SPIN tracking requires relatively long but infrequent time gaps. In the context of GNSS based positioning in NTN, 3GPP has decided to enable the network to configure positioning gaps [49]. SPIN can potentially utilize these gaps for the purpose of periodic tracking. In addition, SPIN can also use other available time gaps such as connected mode discontinuous reception (CDRX). Furthermore, as shown in Fig. 7(a), the tracking windows in successive tracking loops are non-overlapping in this method.

2) Continuous SPIN Tracking: Continuous SPIN tracking maintains the accuracy at a specific level by means of continuous tracking measurements. This method is ideal for the scenario when short time gaps are available frequently during the NTN cellular communication. For instance, in the current NB-IoT standard, the network provides the UEs with 40 ms gaps after every 256 ms of continuous communication for the purpose of resynchronization [51, Ch. 7]. When SPIN operates on an NB-IoT UE, these gaps can be used for tracking. Since SPIN can use the same resynchronization measurements for positioning, it does not affect the resynchronization operation. Similarly, LTE-M UEs are provided with periodic time gaps for neighbor cell measurements [52]. The UE measures the reference signals (RS) in the neighbor cells during these gaps. Since both RS and SSs are present on the acquired signal, SPIN can additionally perform measurements on the SSs during these gaps. Furthermore, in continuous SPIN tracking, the tracking window slides continuously by dropping old stale TOA/FOA measurements and by including fresh TOA/FOA measurements simultaneously. Therefore, the tracking windows in adjacent loops overlap in time, as shown in Fig. 7(b).

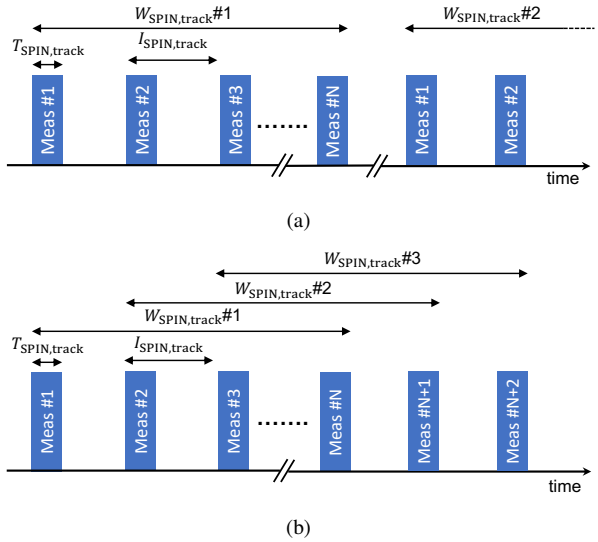

Fig. 7. Timing diagram of (a) Periodic SPIN tracking (b) Continuous SPIN tracking.

Throughout the positioning operation, we assume that the UE velocity does not change significantly during the short positioning windows, $W_{\text{SPIN,acq}}$ and $W_{\text{SPIN,track}}$. While long positioning window gives highly accurate positioning result for UEs with constant velocity, it results in poor accuracy for UEs with changing velocity. Therefore, while choosing $W_{\text{SPIN,acq}}$ and $W_{\text{SPIN,track}}$, one needs to carefully consider the UE mobility aspects and the target accuracy.

IV. Performance Analysis

In the previous section, we defined the detailed steps of SPIN algorithm. In the following, we analyze the performance of SPIN using two key indicators, positioning accuracy and battery life.

A. Positioning Accuracy

We find the theoretical bounds for SPIN positioning accuracy by applying the CRLB [53, Ch. 3]. We do this in two steps: first we find the CRLB for TOA and FOA estimation, and then we use this result to obtain the CRLB for position and velocity estimation using TDOA and FDOA. For the TOA and FOA estimation in SPIN, where the received noisy signal is cross-correlated with a clean template, the CRLB inequalities [54] are given by

$$\sigma_{\text{T}}^2 \geq \frac{1}{8\pi^2\beta^2\frac{E}{N_0}} \tag{31}$$

and

$$\sigma_{\text{F}}^2 \geq \frac{1}{8\pi^2\kappa^2\frac{E}{N_0}}, \tag{32}$$

respectively, where σ_{T}^2 is the variance of the TOA estimation in (18), σ_{F}^2 is the variance of the FOA estimation in (19), E is the energy of $s(t)$ in the time window $T_{\text{SPIN,acq}}$ or $T_{\text{SPIN,track}}$, β is the root mean square (RMS) bandwidth, and κ is the RMS

time of the signal. The RMS bandwidth and time of the signal are define by

$$\beta = \sqrt{\frac{\int_{-\infty}^{\infty} f^2 \left|S(f)\right|^2 df}{\int_{-\infty}^{\infty} \left|S(f)\right|^2 df}} \tag{33}$$

and

$$\kappa = \sqrt{\frac{\int_{-\infty}^{\infty} t^2 \left|s(t)\right|^2 dt}{\int_{-\infty}^{\infty} \left|s(t)\right|^2 dt}}, \tag{34}$$

respectively, where $S(f)$ is the Fourier transform of $s(t)$.

Next, we use the CRLB inequalities in (31) and (32) to fin the CRLB of joint TDOA-FDOA based SPIN position and velocity estimations. While closed-form expressions of TDOA CRLB are given in [55, Ch. 4], we cannot use them since they are meant for 2D positioning and also do not include FDOA. Therefore, for SPIN, we apply the steps provided in the literature [56] for computing TDOA CRLB, and extend that to our scenario of joint TDOA-FDOA based positioning. We consider an estimation problem where we need to estimate $\boldsymbol{\theta}$ from $\boldsymbol{\phi}$. First, we obtain the Fisher information matrix (FIM), $\boldsymbol{J}_{\boldsymbol{\phi}}$, by assuming a Gaussian noise model for intermediate estimates $\boldsymbol{\phi}$ using the variances given in (31) and (32). Since $\boldsymbol{\phi}$ are Gaussian distributed, they have a covariance matrix, $\boldsymbol{C}_{\boldsymbol{\phi}} = \boldsymbol{W}^{-1}$, where $\boldsymbol{W}$ is given in (58). It follows that, the FIM with respect to $\boldsymbol{\phi}$ is given by

$$\boldsymbol{J}_{\boldsymbol{\phi}} = \boldsymbol{C}_{\boldsymbol{\phi}}{}^{-1} = \boldsymbol{W}. \tag{35}$$

The FIM with respect to the fina estimation parameters $\boldsymbol{\theta}$ can be expressed using the chain rule,

$$\boldsymbol{J}_{\boldsymbol{\theta}} = \frac{\partial \boldsymbol{\phi}}{\partial \boldsymbol{\theta}} \boldsymbol{J}_{\boldsymbol{\phi}} \left(\frac{\partial \boldsymbol{\phi}}{\partial \boldsymbol{\theta}}\right)^{\mathrm{T}} = \tilde{\boldsymbol{A}}^{\mathrm{T}} \boldsymbol{J}_{\boldsymbol{\phi}} \tilde{\boldsymbol{A}},$$

where $\tilde{\boldsymbol{A}}$ is given in (55). Finally, the CRLB inequality

$$\boldsymbol{C}_{\hat{\boldsymbol{\theta}}} \geq \left[\boldsymbol{J}_{\boldsymbol{\theta}}^{-1}\right]_{6\times 6}, \tag{36}$$

provides a bound for the covariance matrix $\boldsymbol{C}_{\hat{\boldsymbol{\theta}}}$ of the estimated parameters $\hat{\boldsymbol{\theta}}$. The minimum mean squared error (MMSE) of the estimated position, $\hat{\boldsymbol{X}} = [\hat{x}\ \hat{y}\ \hat{z}]$, and velocity, $\hat{\boldsymbol{V}} = [\hat{v_x}\ \hat{v_y}\ \hat{v_z}]$, can be expressed as

$$E_{\boldsymbol{\theta}} \left\| \boldsymbol{X} - \hat{\boldsymbol{X}} \right\|^2 \geq \left[\boldsymbol{J}_{\boldsymbol{\theta}}^{-1}\right]_{11} + \left[\boldsymbol{J}_{\boldsymbol{\theta}}^{-1}\right]_{22} + \left[\boldsymbol{J}_{\boldsymbol{\theta}}^{-1}\right]_{33} \tag{37}$$

and

$$E_{\boldsymbol{\theta}} \left\| \boldsymbol{V} - \hat{\boldsymbol{V}} \right\|^2 \geq \left[\boldsymbol{J}_{\boldsymbol{\theta}}^{-1}\right]_{44} + \left[\boldsymbol{J}_{\boldsymbol{\theta}}^{-1}\right]_{55} + \left[\boldsymbol{J}_{\boldsymbol{\theta}}^{-1}\right]_{66}, \tag{38}$$

respectively.

B. Battery Life

In the following, we analyze the energy consumption of an NTN IoT UE which uses SPIN for the purpose of UL synchronization. We also provide an analysis for the energy consumption of an NTN IoT UE which uses a GNSS based solution. The energy consumption evaluation helps us to investigate the impact of SPIN on the UE's battery life and also to directly compare the battery life with that of a GNSS based solution. We provide the list of important notations in Table III.

TABLE III
LIST OF IMPORTANT NOTATIONS

Notation	Meaning
P_{TX}	Transmission power
P_{RX}	Reception power
P_{LSL}	Power consumption during light sleep
P_{IDRX}	Power consumption during idle mode discontinuous reception (IDRX) sleep
N_{sat}	Number of satellites visible to the UE
T_{sync}	Sync time
T_{con}	Total duration of RRC connection
$T_{\text{MIB,RX}}$	Master information block (MIB) decoding time
$T_{\text{MIB,idle}}$	Idle time in MIB
$T_{\text{SIB,RX}}$	SIB decoding time
T_{RTT}	RTT between UE and satellite
T_{msg1}	msg1 duration
$T_{\text{msg1,idle}}$	Idle time between msg1 and msg2
T_{msg2}	msg2 duration
T_{msg3}	msg3 duration
T_{msg4}	msg4 duration
$T_{\text{msg4,ACK}}$	msg4 acknowledgement (ACK) duration
$T_{\text{UL,data}}$	UL data duration
$T_{\text{UL,grant}}$	UL grant duration
$T_{\text{UL,RTT}}$	Total round trip wait time between UL data and grants
$T_{\text{DRX-INAT}}$	DRX inactivity timer
T_{CDRX}	CDRX cycle
$T_{\text{CDRX-ON}}$	CDRX-ON duration
T_{IDRX}	IDRX cycle
$T_{\text{IDRX-PO}}$	IDRX paging occasion (PO) duration
$T_{\text{GNSS,acq}}$	GNSS acquisition duration
$T_{\text{GNSS,track}}$	GNSS tracking duration
$T_{\text{GNSS,val}}$	GNSS position validity timer

For the energy consumption analysis, we assume an IoT traffi model where the UE reports UL data periodically at an interval called data reporting interval. Considering the cellular communication protocol fl w given in [18], the total energy consumption per data reporting interval of an NTN IoT UE which performs positioning through SPIN, is given by

$$E_{\text{SPIN}} = \underbrace{P_{\text{RX}}\left(W_{\text{SPIN,acq}} + T_{\text{SPIN,track}} \frac{T_{\text{con}}}{I_{\text{SPIN,track}}}\right)}_{\text{Sync + SPIN positioning}} + N_{\text{sat}} E_{\text{MIB-SIB}} + E_{\text{RA}} + E_{\text{UL}} + E_{\text{CDRX}} + E_{\text{IDRX}}, \tag{39}$$

where $E_{\text{MIB-SIB}}$, E_{RA}, E_{UL}, E_{CDRX}, and E_{IDRX} are the energy consumption associated with MIB and SIB decoding, RA, UL data, CDRX, and IDRX, respectively. The above individual energy components are given by

$$E_{\text{MIB-SIB}} = P_{\text{RX}} T_{\text{MIB,RX}} + P_{\text{LSL}} T_{\text{MIB,idle}} + P_{\text{RX}} T_{\text{SIB,RX}}, \tag{40}$$

$$E_{\text{RA}} = P_{\text{TX}}\left(T_{\text{msg1}} + T_{\text{msg3}} + T_{\text{msg4,ACK}}\right) + 2P_{\text{LSL}} T_{\text{RTT}} + P_{\text{RX}}\left(T_{\text{msg1,idle}} + T_{\text{msg2}} + T_{\text{msg4}}\right), \tag{41}$$

$$E_{\text{UL}} = P_{\text{TX}} T_{\text{UL,data}} + P_{\text{RX}} T_{\text{UL,grant}} + P_{\text{LSL}} T_{\text{UL,RTT}}, \tag{42}$$

$$E_{\text{CDRX}} = P_{\text{RX}} T_{\text{DRX-INAT}} + P_{\text{RX}}\left(N_{\text{CDRX}} T_{\text{CDRX-ON}}\right) + P_{\text{LSL}} N_{\text{CDRX}}\left(T_{\text{CDRX}} - T_{\text{CDRX-ON}}\right), \tag{43}$$

and

$$E_{\text{IDRX}} = P_{\text{IDRX}} N_{\text{IDRX}}\left(T_{\text{IDRX}} - T_{\text{IDRX-PO}}\right) + P_{\text{RX}} N_{\text{IDRX}} T_{\text{IDRX-PO}}, \tag{44}$$

where N_{CDRX} and N_{IDRX} represent the number of CDRX and IDRX cycles, respectively, which are decided by the values of data inactivity ($T_{\text{data-INAT}}$) and T_{3324}[3] timers, respectively [57]–[59]. For periodic SPIN tracking, $I_{\text{SPIN,track}} = T_{\text{SPIN,val}}$ in (39). Note that when SPIN is used to get position fi for the purpose of UL sync, UE operations associated with establishing RRC connection are done only once per reporting interval. However, SPIN requires extra synchronization measurements from one or more satellites as it uses SSs for positioning purposes.

As explained in Section I, recall 3GPP's working assumption that the IoT UEs are incapable of performing both GNSS and cellular operations simultaneously. Based on this assumption, for the GNSS based solution, the total energy consumption per data reporting interval is given by

$$E_{\text{GNSS}} = \underbrace{P_{\text{RX}}\left(T_{\text{GNSS,acq}} + N_{\text{GNSS}}\, T_{\text{GNSS,track}}\right)}_{\text{GNSS positioning}}, \tag{45}$$
$$+ N_{\text{GNSS}}\left(E_{\text{sync}} + E_{\text{MIB-SIB}} + E_{\text{RA}}\right) + E_{\text{UL}} + E_{\text{CDRX}} + E_{\text{IDRX}},$$

where E_{sync} is the energy consumption associated with cellular synchronization, given by

$$E_{\text{sync}} = P_{\text{RX}} T_{\text{sync}}, \tag{46}$$

and N_{GNSS} represents the number of times GNSS positioning is required in each reporting interval, given by

$$N_{\text{GNSS}} = \frac{T_{\text{con}}}{T_{\text{GNSS,val}}}. \tag{47}$$

We see from (45) that the UE operations associated with establishing cellular connection such as synchronization, RA, and MIB and SIB decoding are performed N_{GNSS} times. This is because the IoT UEs do not have the capability to simultaneously perform cellular and GNSS operations. The UE terminates RRC connection and enters RRC idle mode before GNSS positioning.

Based on the above energy consumption analysis, we now defin the battery life of both SPIN and GNSS based solutions. Let the data reporting interval of the UE be I_{rep} hours and the UE battery capacity be E_{b} Wh. Then, the battery life, in years, of an NTN-IoT UE using SPIN and GNSS based solutions are given by

$$L_{\text{SPIN}} = \frac{E_{\text{b}} \times 60 \times 60}{E_{\text{SPIN}} \frac{24\times 365}{I_{\text{rep}}}} \tag{48}$$

and

$$L_{\text{GNSS}} = \frac{E_{\text{b}} \times 60 \times 60}{E_{\text{GNSS}} \frac{24\times 365}{I_{\text{rep}}}}, \tag{49}$$

respectively, where E_{SPIN} and E_{GNSS} are in units of J.

In the next section, we provide the numerical results for SPIN accuracy compared with the corresponding CRLB, the SPIN battery life compared with that of GNSS based solution, and the computational complexity of SPIN.

[3] T_{3324} timer starts when the UE enters IDRX mode which consists of periodic paging cycles, and upon the expiry of the timer, it transitions into deep sleeping power saving mode (PSM) [57]

V. Numerical Results

In the above, we discussed the theoretical bounds of the SPIN positioning accuracy and provided the analytical equations for battery life comparison of a UE using SPIN with that of GNSS. In this section, we perform PHY and system level simulations of SPIN to obtain the achieved positioning accuracy and compare that with the corresponding CRLB. For the same evaluation settings, we also provide numerical results of battery life savings in an IoT UE which uses SPIN instead of GNSS based solution. Finally, we show the computational complexity of SPIN in terms of the number of operations and memory requirements.

A. Simulation Settings

For both positioning accuracy and battery life evaluations, we choose the evaluation parameters and their values from the relevant 3GPP technical documents and reports [18], [59], [60]. We list the parameters and their values we use for our evaluations in Table IV. We adopt all the time parameters in the protocol fl w and their values from [18], and hence we do not repeat them in Table IV. We choose SPIN-specifi measurement time parameters such as the acquisition and tracking durations, windows, and intervals based on a trial and error approach to fin the values required to achieve the target requirements for UL synchronization. To achieve global coverage, we select a satellite constellation of sufficien size which is comparable with that of currently planned and/or deployed LEO constellations such as Starlink [19], [20] and Amazon-Kuiper [20]. To evaluate the worst case which corresponds to deep coverage, we perform both SPIN accuracy and battery life evaluations at an MCL of 164 dB. Further, we choose set-4 satellite beam configuratio for which the link budget matches with 164 dB MCL [18], [61]. For the sake of conciseness, we provide SPIN evaluation for only NB-IoT standard. Nevertheless, the evaluations can be extended in a similar way to LTE-M standard.

For the simulations, we apply the NTN channel models recommended by 3GPP [2]. Considering the application scenarios, the NTN is not necessary for UEs located in urban environments since they are mostly under cellular coverage. On the other hand, suburban, rural, and open-sky environments are ideal application scenarios where NTN support is critical. While an open-sky environment always guarantees LOS signals and hence results in better positioning accuracy, suburban and rural scenarios are characterized by NLOS probabilities depending on the associated elevation angle [2]. To evaluate the worst case among the relevant scenarios, we choose the channel model parameters corresponding to a suburban environment. The channel model includes small scale fading, which emulates the multipath effect mainly caused by the obstacles close to the UE, and the Doppler spread due to the UE motion [2]. The SNR is obtained from the NTN IoT link budget [1], [18] as

$$\gamma = \frac{P_{\text{EIRP}} G}{B k_{\text{B}} T \alpha_{\text{fs}} \alpha_{\text{atm}} \alpha_{\text{sh}} \alpha_{\text{sc}} \alpha_{\text{pol}} \alpha_{\text{add}}}, \tag{50}$$

TABLE IV
SIMULATION SETTINGS

Parameter	Value	Parameter	Value
Positioning Evaluation Settings			
Channel	NTN TDL-D	LEO height	600 km
Constellation	87.5°:2400/40/20	Standard	NB-IoT
Coherent time	1 ms	Environment	Suburban
Beam configuratio	Set-4	f_s	1.92 Msps
Minimum elevation	30°	UE speed	120 km/h
$k_{\max}$ (acquisition)	10 for parallel, 30 for sequential	MCL	164 dB
		No. of UEs	1000
$k_{\max}$ (tracking)	20 for parallel, 40 for sequential	ϵ_{th}	0.0001
		$T_{\text{SPIN,proc}}$	100 ms
Battery Evaluation Settings			
E_{b}	5 Wh	T_{CDRX}	640 ms
P_{TX}	543 mW	$T_{\text{CDRX-ON}}$	100 ms
P_{RX}	37 mW	T_{IDRX}	1.28 s
P_{LSL}	8.75 mW	$T_{\text{IDRX-PO}}$	100 ms
P_{IDRX}	105 μW	T_{3324}	16 s
N_{sat}	8	$T_{\text{GNSS,acq}}$	1-30 s
T_{RTT}	26 ms	$T_{\text{GNSS,track}}$	1 s
$T_{\text{DRX-INAT}}$	100 ms	$T_{\text{GNSS,val}}$	6.4 s
$T_{\text{data-INAT}}$	5 s	I_{rep}	2, 24 h
$T_{\text{SPIN,val}}$	5.9 s	Data size	200 bytes
Common Settings			
$W_{\text{SPIN,acq}}$	1.1 s for parallel, 5.2 s for sequential	$I_{\text{SPIN,acq}}$	215 ms
		$I_{\text{SPIN,track}}$	296 ms
$W_{\text{SPIN,track}}$	296 ms for parallel, 2.1 s for sequential	$T_{\text{SPIN,acq}}$	215 ms
		$T_{\text{SPIN,track}}$	40 ms

where P_{EIRP} is the effective isotropic radiated power (EIRP) from the satellite, G/T is the antenna-gain-to-noise-temperature of the UE, B is the bandwidth of the synchronization signal, k_{B} is the Boltzmann constant, α_{atm} is the atmospheric path loss, α_{sh} is the shadowing margin, α_{sc} is the scintillation loss, α_{pol} is the polarization loss, α_{add} includes all other additional losses, and α_{fs} is the free space path loss [2] given by

$$\alpha_{\text{fs}} = (4\pi f_c d/c)^2, \tag{51}$$

where d is the distance between the satellite and the UE.

The number of synchronization measurements that a UE can perform in an acquisition or tracking window depends heavily on the network implementation. This includes factors such as the partition of available network bandwidth into intra- and inter-frequency cells and the deterministic time offset between the cells. Therefore, we assume two extreme cases for our evaluations. First, we evaluate the worst case where the UE can only sequentially acquire synchronization measurements from one cell to another. The worst case corresponds to a scenario where all the available synchronization signals in the SPIN window belong to inter-frequency cells. However, it might be possible for a UE with adequate processing capability to measure synchronization signals from multiple intra-frequency cells in the acquisition bandwidth simultaneously, if they are time multiplexed. Therefore, we also evaluate the best case, i.e., with parallel measurements, where the UE can simultaneously acquire all available synchronization measurements in a SPIN window. SPIN takes longer time to get position fi when acquiring SSs sequentially. Therefore, for sequential method, we choose acquisition and tracking windows longer than that of parallel method.

For battery life comparison and computational complexity evaluation, we use the same values of time parameters which we used for SPIN accuracy evaluation. For estimating the battery life of a UE using GNSS based solution, we choose GNSS acquisition and tracking durations from 3GPP technical report [18]. Without loss of generality, we use the term GNSS throughout our evaluations to indicate GPS, which is the widely used GNSS service. Finally, to maintain low computational complexity along with reasonably high accuracy, we set $T_{\text{SPIN,proc}}$ to 100 ms.

B. Methodology

We perform the SPIN accuracy evaluation in two steps: evaluation of i) TOA and FOA estimation using PHY simulation, ii) position and velocity estimation using system level simulation, and compare with the corresponding CRLBs.

In the firs step, using MATLAB LTE and 5G Toolbox, we generate SSs, pass them through the NTN channel models, and estimate TOA and FOA. To account for the non-line-of-sight (NLOS) paths in a suburban environment, we apply a penalty by disregarding NLOS signals based on the LOS-NLOS probability given in [2]. In our evaluations, we assume that the UE filter out the NLOS signals, which can be done based on the signal strength as explained in [7].

In the second step, we conduct system level simulations of SPIN acquisition and tracking, by considering a satellite constellation and a set of UEs located on the earth. Note that the evaluation models in the existing work on NTN NR positioning [7] do not consider the impact of true UE location on the achieved accuracy. In reality, the achievable accuracy varies significantl depending on the true UE location. To this end, to fully capture the impact of all locations, we consider uniformly spaced 1000 UEs on the earth. However, for a near-polar Walker-star constellation, over-crowding of satellites happens at the poles. In reality, some of the satellites turn off their beams in a coordinated manner to avoid high interference at those regions [62]. In effect, the polar UEs will experience satellite and beam visibility very similar to that of the UEs located anywhere else. Consequently, we expect that the selected satellite beams will result in polar UEs having similar SPIN accuracy compared to other UEs. Rather than implementing an arbitrary pattern of selective beam disabling, we simply exclude the polar regions which is also an easier choice from the simulation perspective. Regardless of the above simulation assumption, SPIN is applicable to UEs located anywhere on the earth. Furthermore, our simulation model accounts for the significan variation of SNR during the satellite fly-b , thus ensuring accurate simulation results. To this end, we calculate SNR using (50) for each measurement and apply noise variance separately, instead of setting a fi ed variance for the noise in all measurements.

C. Positioning Evaluation

1) Fine Time and Frequency Offset Estimation: We firs evaluate TOA and FOA estimation accuracy using PHY simulation of PSS and SSS in NTN channel for the range of SNR given by the NTN IoT link budget. We compare these

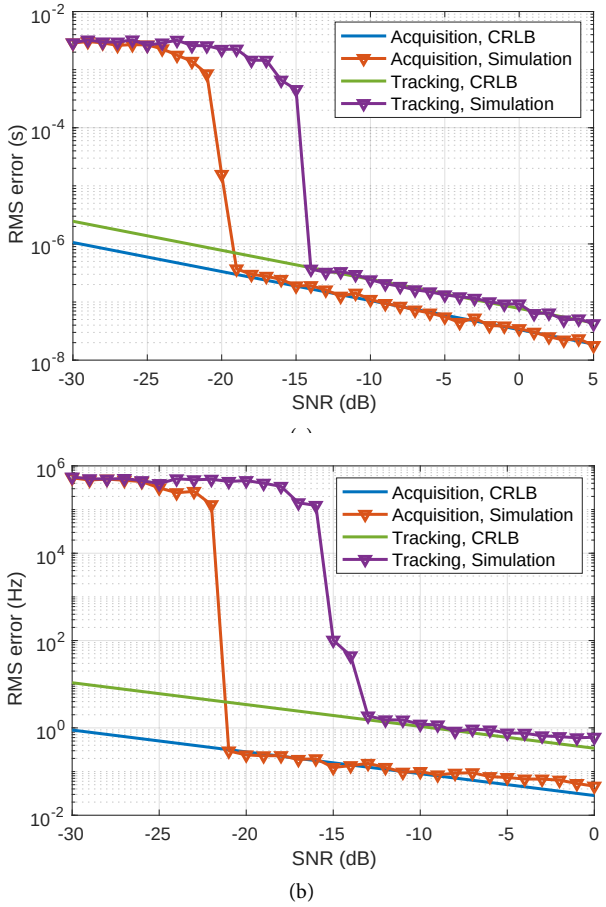

(b)

Fig. 8. (a) TOA (b) FOA estimation errors compared with corresponding CRLBs.

simulation results with the corresponding CRLB in Fig. 8. The SNR for 164 dB MCL ranges from -12 to -7 dB when the satellite moves from the minimum to the maximum elevation angles of 30° to 90°, respectively. The results in Fig. 8 show that the TOA and FOA estimated using correlation over the chosen acquisition and tracking durations followed by fin resolution curve fittin approach the CRLB for the concerned range of SNR. Only under very low SNR, both the TOA and FOA estimations fail due to an unavoidable anomalous behavior [63]. This occurs outside the asymptotic region of CRLB and thus cannot be bounded by the CRLB accurately [64]. However, considering that the possible SNR range for the NTN scenario is within the asymptotic region, we can still rely on CRLB as the lower bound in our simulation. Additionally, at very high SNR, the TOA and FOA estimations tend to saturate thus creating gaps with CRLB. This saturation is due to the estimation bias caused by the small scale fading in the channel.

2) Position and Velocity Estimation: In the above, we showed that the TOA and FOA estimations in SPIN achieve the corresponding CRLB s for the concerned range of SNR. Therefore, for the following SPIN acquisition and tracking simulations, we assume that the TOA/FOA measurements have Gaussian distributions with mean and variance equal to the true TOA/FOA values and CRLB, respectively. For uniformly

TABLE V
90TH PERCENTILE RMS ERROR OF POSITION AND VELOCITY

Measurement Type	Positioning Step	Position (m)		Velocity (m/s)	
		CRLB	Simulation	CRLB	Simulation
Parallel	Acquisition	17.4	20.6	0.1	0.8
	Tracking	188.4	207.3	1.7	4.9
Sequential	Acquisition	15.9	18.2	0.1	0.4
	Tracking	193.9	212.6	2.0	3.1

spaced 1000 UEs on the earth, we show the 90th percentile of RMS error in SPIN position and velocity and their comparison with the corresponding CRLBs, in Table V. We see that in all cases, SPIN results are close to the position and velocity CRLBs. As given in Table IV, we set the number of TWLS iterations to small values to have low computational complexity. However, if we run SPIN for more TWLS iterations, the position and velocity accuracy approach the corresponding CRLBs, but at the expense of a higher computational complexity. It should be noted that SPIN acquisition achieves the target requirements shown in Fig. 4 for a wide range of error budget covering low to very high oscillator errors. On the other hand, we choose reasonably short SPIN tracking window such that the results just meet the target requirements for $80-20\%$ error budget. However, to get higher accuracy, SPIN tracking window can be cautiously increased, provided that the assumption of UE velocity remaining constant during the entire window remains valid. To better investigate the overall performance of SPIN for the entire distribution of UEs, we have also plotted an empirical cumulative density function (CDF) of the RMS position and velocity error in Fig. 9. As expected, the CDF of the acquisition error is consistently lower than that of the tracking. The 90th percentile of the position and velocity errors are consistent with the results which we showed in Table V. In Fig. 9, we also observe that majority of the UEs experience much lower RMS positioning errors compared to the target requirements discussed in Section II. To make it concise, in the above, we showed the results for only sequential measurements scenario. However, the trend is similar in the parallel measurements case too.

In Table V and Fig. 9, we showed SPIN accuracy results for stand-alone acquisition and tracking operations by configurin appropriate durations. To show the real-time accuracy variation starting from SPIN acquisition until a few loops of SPIN tracking, we have also plotted the 90th percentile of RMS error against time in Fig. 10. For the sake of conciseness, we show the results for only sequential measurements case here. However, we see a similar trend in the parallel measurements scenario too. For continuous tracking, the accuracy of both position and velocity initially reduce over time before finall saturating to a level. This is because SPIN maintains a sliding tracking window which discards old measurements while including new measurements. The TOA and FOA measurements performed during the initial acquisition are superior than the tracking measurements due to the longer acquisition duration and hence give higher accuracy. Until the acquisition-tracking boundary as shown in Fig. 10, the set of measurements include at least one measurement from the initial acquisition. However, afterwards, the accuracy remains approximately same since

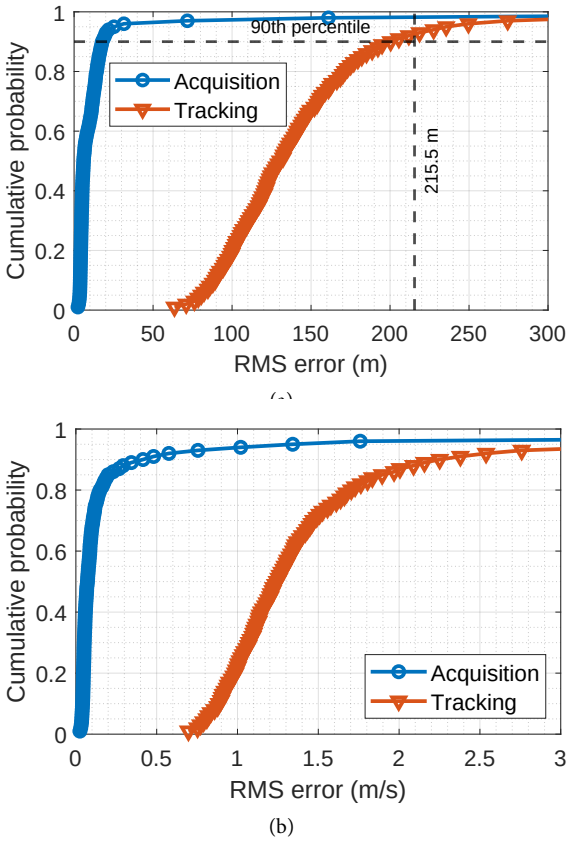

Fig. 9. Empirical CDF of (a) position (b) velocity estimation errors, for sequential measurements case.

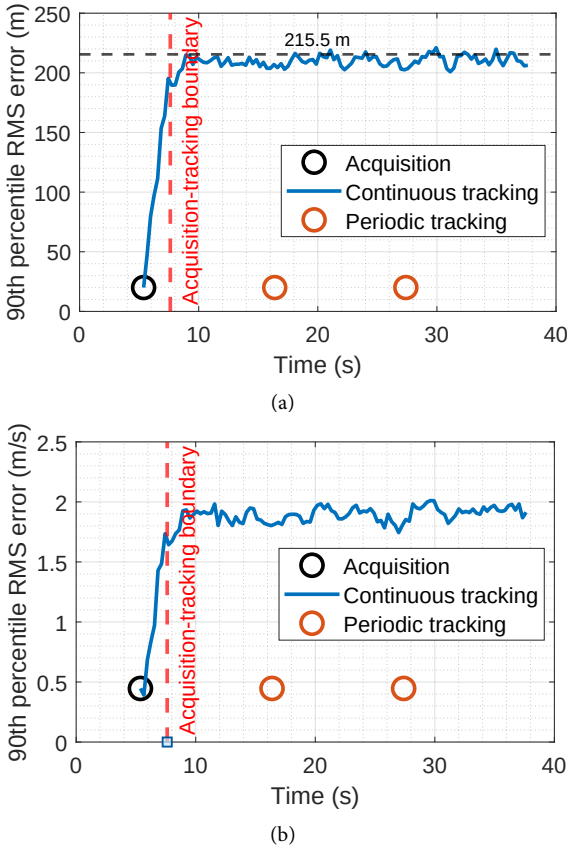

Fig. 10. 90th percentile RMS error of (a) position and (b) velocity estimation vs. time, for sequential measurements case.

the following tracking measurements are performed with a fi ed duration and interval. We observe that, SPIN maintains position and velocity RMS error below 215 m and 2 m/s, respectively, by performing measurements every 296 ms. On the other hand, in periodic tracking, SPIN gets a position fi every time when $T_{\text{SPIN,val}}$ expires. In our simulations, we set $T_{\text{SPIN,val}}$ based on the value of UE speed. Since the UE is moving, the error relative to the previous estimated position increases over time. In this regard, we set $T_{\text{SPIN,val}}$ equal to the time taken for the position error to reach 215 m, which is the allowed position error for $80-20\%$ error budget in Fig. 4. For continuous tracking, the values of tracking window, interval, and duration used in the simulations are specifie in Table IV. However, periodic SPIN tracking measurement parameters need to be similar to that of acquisition measurement as they require high accuracy. Therefore, for periodic tracking, we set $W_{\text{SPIN,track}}$, $I_{\text{SPIN,track}}$, and $T_{\text{SPIN,track}}$ equal to the values of $W_{\text{SPIN,acq}}$, $I_{\text{SPIN,acq}}$, and $T_{\text{SPIN,acq}}$ given in Table IV, respectively. The circles in Fig. 10 represent the accuracy achieved by SPIN acquisition followed by periodic tracking. Since we set the tracking window long enough to get highly accurate position, the periodic tracking accuracy remains valid until the expiry of $T_{\text{SPIN,val}}$. Recall that we chose the SPIN measurement time parameters for our simulations based on the target accuracy requirement. Our intention is not to achieve the best accuracy on par with, say, GNSS, instead we aim to just achieve the target requirements for UL synchronization along with minimum energy consumption and computational complexity. Alternatively, if SPIN is applied on a different use-case than the UL synchronization, e.g., LBS, one can tune the measurement time parameters to achieve higher accuracy. However, the improved accuracy comes at the cost of higher energy consumption and computational complexity in the UE.

As already mentioned in Section II, UE velocity related Doppler offset in the UL is taken care by the network. However, given the high accuracy of UE velocity estimation in SPIN, the IoT UE can additionally pre-compensate the UL signal for the UE Doppler.

D. Battery Life Comparison

First, we compare the total energy consumption per reporting interval of an IoT UE which uses SPIN with that of a UE using GNSS, in Fig. 11(a). The time to get a GNSS position fi varies based on a range of factors including the type of chipset, the positioning interval, and the visibility to GNSS satellites. To this end, for $I_{\text{rep}} = 2$ h, we vary the GNSS acquisition duration, $T_{\text{GNSS,acq}}$, from 1 to 5 s where GNSS performs a hot-start positioning [18]. On the other hand, GNSS performs a cold-start positioning when $I_{\text{rep}} = 24$ h, and hence we vary $T_{\text{GNSS,acq}}$ from 5 to 30 s [18]. We see in Fig. 11(a) that, for the entire range of $T_{\text{GNSS,acq}}$, GNSS based solution consumes more energy than SPIN. This is mainly because of repeated termination and re-establishment of RRC

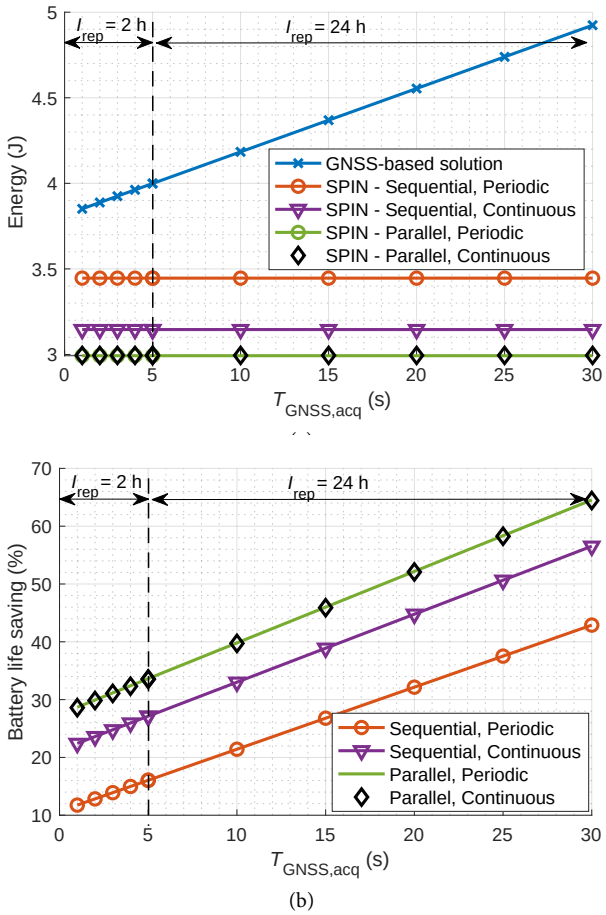

Fig. 11. (a) Comparison of energy consumption per reporting interval of SPIN with GNSS based solution. (b) Battery life saving with SPIN.

connection associated with the GNSS positioning gaps. On the other hand, SPIN is capable of performing positioning in a time-multiplexed manner without interrupting the underlying cellular communication. This results in significantl less energy consumption associated with SPIN. Further, we see that the energy consumption in GNSS based solution increases with increase in $T_{\text{GNSS,acq}}$, since longer duration of GNSS reception is performed for higher $T_{\text{GNSS,acq}}$. On the other hand, the energy consumption in SPIN remains constant for all combinations of settings, since it is independent of $T_{\text{GNSS,acq}}$. SPIN consumes more energy when it performs sequential measurements than when it performs parallel measurements. This is because SPIN performs reception of SSs for longer duration when it performs measurements sequentially. For the sequential measurement case, periodic SPIN tracking consumes more energy than continuous SPIN tracking. The reason is that we set the periodic tracking duration to a large value to get high accuracy which should remain valid until the expiry of $T_{\text{SPIN,val}}$. However, continuous tracking maintains the accuracy within an acceptable limit by making use of short and frequent time gaps, thus consuming less energy. This changes for the parallel measurement case, in which the energy consumptions for periodic and continuous tracking are approximately the same. This is because of the same effective reception duration of SS measurements for the chosen settings.

Finally, we show the battery life saving associated with SPIN over the GNSS-based solution in Fig. 11(b). For the best case where SPIN performs parallel measurements, it saves around $29-64\%$ of the UE's battery life. Even in the worst case where sequential measurements are performed, SPIN offers a significan battery life saving which ranges from 12 to 43%. Like we explained in the context of energy consumption results, the significan battery life saving achieved by SPIN also owes to its capability to perform positioning without interrupting the cellular connection.

TABLE VI
COMPUTATIONAL COMPLEXITY OF SPIN

Positioning Step	Number of Operations			
	Parallel Acquisition	Sequential Acquisition	Parallel Tracking	Sequential Tracking
Curve Fitting	640	384	128	112
2-WLS	500702	153144	-	-
TWLS	1294950	1095030	77620	124280
MOPS	17.96	12.48	0.78	1.24

E. Computational Complexity

We show the number of basic arithmetic operations associated with SPIN acquisition and tracking for both parallel and sequential measurements scenarios in Table VI. The number of operations in TWLS includes all the computations performed during the entire iterative process until the convergence. Using the number of operations and $T_{\text{SPIN,proc}}$, we calculate the computational complexity in terms of million operations per second (MOPS). For SPIN acquisition, the MOPS associated with parallel measurements case is higher than that of sequential measurements. Therefore, for an NB-IoT UE with low complexity, SPIN acquisition with sequential measurements is more suitable. On the other hand, an LTE-M UE with higher computational capacity can perform SPIN acquisition with parallel measurements which can achieve sufficien accuracy in shorter measurement time. The evaluations also show that MOPS required for both sequential and parallel measurement cases in SPIN tracking are lower than that of acquisition since tracking is performed with less number of measurements. The most computationally demanding cases in NB-IoT are data channel processing and SS detection which require 18.5 and 30 MOPS, respectively [51]. We see that the MOPS in both parallel and sequential cases of SPIN are much lower than the MOPS required by the existing computationally expensive cases. For the above evaluation, we did not consider the operations associated with the coarse synchronization step since SPIN directly reuses the results from the cellular operation. As the cellular UE has the computational capacity to perform correlation on signals at same sampling rate and comparable lengths as part of fin synchronization, we also do not analyze the complexity associated with the subsequent SPIN correlation operations.

We also computed the memory requirement in the UE for performing SPIN, which is mainly decided by the size of the matrices involved in 2-WLS and TWLS steps. The highest memory requirement is for parallel SPIN acquisition which needs 28 kB of storage space. On the other hand,

sequential SPIN tracking takes only 1 kB of memory. This is not significant for IoT UEs which usually have a random access memory (RAM) size of 256 kB [65], [66].

It should be noted that, in the battery life analysis, we did not consider the power consumption associated with the computations related to SPIN, GNSS, or cellular operations. For even a relatively less efficient processor with an efficiency of 144 MOPS/mW [67, Ch. 5], the power consumption associated with the computations in SPIN parallel acquisition, the most computationally demanding case, is only 0.1 mW. However, for a superior processor efficiency of 970 MOPS/mW, the power consumption further reduces to 18 μW. Therefore, it is meaningful to assume that the SPIN computations have negligible impact on the battery life of the UE.

VI. Discussion

In this section, we provide brief qualitative analysis of SPIN in additional scenarios which are not evaluated in the paper.

A. LTE-M

In the above, we evaluated SPIN for NB-IoT standard where it uses NPSS and NSSS for positioning. In a similar way, we can evaluate SPIN for the LTE-M standard by replacing NPSS and NSSS with PSS and SSS, respectively. In contrast to NB-IoT, LTE-M is meant to support lower coverage level and hence we can consider an MCL of 154 dB, which corresponds to set-3 or set-2 beam configurations [18], [61]. For the LTE-M standard, which uses PSS and SSS with a bandwidth higher than that of NPSS and NSSS, we observe that the SPIN accuracy is much higher than that of NB-IoT.

B. Reduced Constellation Size

The satellite constellation chosen for our evaluation gives visibility to more than one satellite at any instant of time to every UE. Nevertheless, SPIN also works in those scenarios where there is limited visibility, e.g., a constellation consisting of 510 LEO satellites at an altitude of 600 km, which is the minimum constellation size for global coverage [32]. However, in a limited visibility scenario, SPIN takes a longer duration to get an accurate position fix

C. Indoor Scenario

We considered outdoor UEs for the SPIN evaluations in this paper. However, SPIN also works in soft indoor cases, where an additional loss needs to be included in the link budget, e.g., 9 dB [61]. However, for deep indoor cases which suffer from severe outdoor-to-indoor (O2I) losses, the link budget as per the satellite reference parameters defined by 3GPP [1], [18] is insufficient Alternatively, if LEO satellites with higher antenna gain are deployed, successful UL and DL communication are possible for deep indoor cases [13]. In such a scenario, SPIN can operate successfully in an NTN UE and can provide position fix to resolve UL synchronization issues and to serve LBS.

D. Other Environments

For the evaluations in this paper, we considered an NTN channel in a suburban environment with LOS probability as defined in [2]. In an open-sky environment, e.g., when the UEs are mounted on aircrafts or boats, we can assume an AWGN channel with 100% LOS possibility. On the other hand, in an urban or dense urban environment, the LOS probability is lower than that of a suburban scenario. Nevertheless, our evaluations can be directly extended to the above cases. We see that the accuracy in open-sky environment is better than the suburban scenario which we evaluated in our paper. However, the accuracy will be lower in an urban environment due to the lower LOS probability. This is not a major concern since the IoT UEs located in urban environment are more likely to be served by the terrestrial cellular BSs.

VII. Conclusion

SPIN enables self-positioning in NTN IoT UEs for the purpose of solving the UL synchronization problem and to provide LBS. SPIN performs positioning by utilizing TDOA and FDOA measurements on the existing DL SSs, thus requiring no network modification SPIN adopts widely accepted signal processing techniques that are already proved to yield good performance. The theoretical achievability of the target accuracy using the available signals and measurements is determined based on the CRLB for TOA, FOA, position, and velocity estimations. The numerical results demonstrate that SPIN indeed meets the target accuracy required for the UL synchronization problem while achieving the CRLB. Our analysis also shows significant battery life savings when a GNSS-based solution is replaced with SPIN. Further, the computational complexity associated with SPIN is much lower than that of the existing cellular operations. The computational complexity and positioning accuracy analyses help us to decide on the appropriate accuracy-complexity tradeoff for a selected use-case. Since SPIN also estimates the UE velocity with high accuracy, the UE can additionally compute and compensate the Doppler caused by its own mobility thereby relieving the network from doing the same. The positioning accuracy, the battery life analyses, and the low complexity prove that SPIN is an appealing solution for the UL sync problem in NTN IoT UEs. Further, the analyses, the evaluation methodology, and the results presented in this paper will help any future research in the area of IoT NTN. A potential future research could be conducted on optimizing the continuous synchronization operations that can enable more efficient SPIN tracking and thus leads to a reduction of overall computational complexity in the UE.

Appendix

Using Taylor series first order approximation, any nonlinear multivariable function $q(x, y, \ldots)$, which is differentiable at $[x_0, y_0, \ldots]$ can be expressed in linear form as

$$q(x, y, \ldots) = q(x_0, y_0, \ldots) + \left[\left.\frac{\partial q}{\partial x}\right|_{(x_0, y_0, \ldots)} \left.\frac{\partial q}{\partial y}\right|_{(x_0, y_0, \ldots)} \ldots \right]$$

$$\times \left[x - x_0 \; y - y_0 \ldots\right]^{\mathrm{T}}. \tag{52}$$

Using (52), $f_i(\boldsymbol{X}, \boldsymbol{V})$ and $g_i(\boldsymbol{X}, \boldsymbol{V})$ in (26) and (27) can be expressed in linear form, which results in a set of $2(N-1)$ linear equations that can be represented in the form of (29). The matrices $\boldsymbol{A}$ and $\boldsymbol{B}$ in (29) and (30) are given by

$$\boldsymbol{A} = \tilde{\boldsymbol{A}}\Big|_{\boldsymbol{X}=\boldsymbol{X}_0, \boldsymbol{V}=\boldsymbol{V}_0} \tag{53}$$

and

$$\boldsymbol{B} = \begin{bmatrix} r_{21} - (R_2 - R_1) \\ \vdots \\ r_{N\;N-1} - (R_N - R_{N-1}) \\ \dot{r}_{21} - (\dot{R}_2 - \dot{R}_1) \\ \vdots \\ \dot{r}_{N\;N-1} - (\dot{R}_N - \dot{R}_{N-1}) \end{bmatrix} + \boldsymbol{A}[\boldsymbol{X}_0 \; \boldsymbol{V}_0]^{\mathrm{T}}, \tag{54}$$

respectively, where

$$\tilde{\boldsymbol{A}} = \begin{bmatrix} \frac{\partial(f_2 - f_1)}{\partial x} & \frac{\partial(f_2 - f_1)}{\partial y} & \cdots & \frac{\partial(f_2 - f_1)}{\partial v_z} \\ \vdots & \vdots & \ddots & \vdots \\ \frac{\partial(f_N - f_{N-1})}{\partial x} & \frac{\partial(f_N - f_{N-1})}{\partial y} & \cdots & \frac{\partial(f_N - f_{N-1})}{\partial v_z} \\ \frac{\partial(g_2 - g_1)}{\partial x} & \frac{\partial(g_2 - g_1)}{\partial y} & \cdots & \frac{\partial(g_2 - g_1)}{\partial v_z} \\ \vdots & \vdots & \ddots & \vdots \\ \frac{\partial(g_N - g_{N-1})}{\partial x} & \frac{\partial(g_N - g_{N-1})}{\partial y} & \cdots & \frac{\partial(g_N - g_{N-1})}{\partial v_z} \end{bmatrix}, \tag{55}$$

$$R_i = f_i(\boldsymbol{X} = \boldsymbol{X}_0, \boldsymbol{V} = \boldsymbol{V}_0), \tag{56}$$

and

$$\dot{R}_i = g_i(\boldsymbol{X} = \boldsymbol{X}_0, \boldsymbol{V} = \boldsymbol{V}_0), \tag{57}$$

respectively. The weight matrix $\boldsymbol{W}$ is ideally a function of the covariance matrix of the measurements, given by

$$\boldsymbol{W} = \begin{bmatrix} c^2 \boldsymbol{W}_{\mathrm{TDOA}}^{-1} & \boldsymbol{0}_{N-1 \times N-1} \\ \boldsymbol{0}_{N-1 \times N-1} & \frac{c^2}{f_c^2} \boldsymbol{W}_{\mathrm{FDOA}}^{-1} \end{bmatrix}^{-1}, \tag{58}$$

where $\boldsymbol{W}_{\mathrm{TDOA}}^{-1}$ and $\boldsymbol{W}_{\mathrm{FDOA}}^{-1}$ are given by

$$\boldsymbol{W}_{\mathrm{TDOA}}^{-1} = \tag{59}$$
$$\begin{bmatrix} \sigma_{\mathrm{T},2}^2 + \sigma_{\mathrm{T},1}^2 & \sigma_{\mathrm{T},2}^2 & 0 & \cdots & 0 \\ \sigma_{\mathrm{T},2}^2 & \sigma_{\mathrm{T},3}^2 + \sigma_{\mathrm{T},2}^2 & \sigma_{\mathrm{T},3}^2 & \cdots & 0 \\ 0 & \sigma_{\mathrm{T},3}^2 & \sigma_{\mathrm{T},4}^2 + \sigma_{\mathrm{T},3}^2 & \cdots & 0 \\ \vdots & \vdots & \vdots & \ddots & \vdots \\ 0 & 0 & 0 & \cdots & \sigma_{\mathrm{T},N}^2 + \sigma_{\mathrm{T},N-1}^2 \end{bmatrix}$$

and

$$\boldsymbol{W}_{\mathrm{FDOA}}^{-1} = \tag{60}$$
$$\begin{bmatrix} \sigma_{\mathrm{F},2}^2 + \sigma_{\mathrm{F},1}^2 & \sigma_{\mathrm{F},2}^2 & 0 & \cdots & 0 \\ \sigma_{\mathrm{F},2}^2 & \sigma_{\mathrm{F},3}^2 + \sigma_{\mathrm{F},2}^2 & \sigma_{\mathrm{F},3}^2 & \cdots & 0 \\ 0 & \sigma_{\mathrm{F},3}^2 & \sigma_{\mathrm{F},4}^2 + \sigma_{\mathrm{F},3}^2 & \cdots & 0 \\ \vdots & \vdots & \vdots & \ddots & \vdots \\ 0 & 0 & 0 & \cdots & \sigma_{\mathrm{F},N}^2 + \sigma_{\mathrm{F},N-1}^2 \end{bmatrix},$$

respectively, where $\sigma_{\mathrm{T},i}^2$ and $\sigma_{\mathrm{F},i}^2$ are the variance of estimation errors in ith TOA and FOA measurements as indicated in (31) and (32), respectively. However, in practice, the covariance matrix is unknown. For SPIN, since we have rough position and velocity estimates obtained from 2-WLS, we use them to compute initial value of $\boldsymbol{W}$. We update $\boldsymbol{W}$ after each TWLS iteration based on the updated position and velocity estimates.

References

[1] TR 38.821 V1.0.0, "Solutions for NR to support non-terrestrial networks (NTN) (Release 16)," 3rd Generation Partnership Project (3GPP), Tech. Rep., Dec. 2019.

[2] TR 38.811 V15.2.0, "Study on New Radio (NR) to support non-terrestrial networks (Release 15)," 3rd Generation Partnership Project (3GPP), Tech. Rep., Sept. 2019.

[3] F. Rinaldi, H.-L. Maattanen, J. Torsner, S. Pizzi, S. Andreev, A. Iera, Y. Koucheryavy, and G. Araniti, "Non-terrestrial networks in 5G & beyond: A survey," *IEEE Access*, vol. 8, pp. 165 178–165 200, Sept. 2020.

[4] M. Vaezi, A. Azari, S. R. Khosravirad, M. Shirvanimoghaddam, M. M. Azari, D. Chasaki, and P. Popovski, "Cellular, wide-area, and non-terrestrial IoT: A survey on 5G advances and the road toward 6G," *IEEE Commun. Surveys Tuts.*, vol. 24, no. 2, pp. 1117–1174, Feb. 2022.

[5] O. Liberg, S. E. Löwenmark, S. Euler, B. Hofström, T. Khan, X. Lin, and J. Sedin, "Narrowband internet of things for non-terrestrial networks," *IEEE Commun. Standards Mag.*, vol. 4, no. 4, pp. 49–55, Dec. 2020.

[6] A. Wang, P. Wang, X. Miao, X. Li, N. Ye, and Y. Liu, "A review on non-terrestrial wireless technologies for smart city internet of things," *Int. J. Distrib. Sensor Netw.*, vol. 16, no. 6, 2020.

[7] F. Zhu, T. Ba, Y. Zhang, X. Gao, and J. Wang, "Terminal location method with NLOS exclusion based on unsupervised learning in 5G-LEO satellite communication systems," *Int. J. Satell. Commun. Netw.*, vol. 38, no. 5, pp. 425–436, Feb. 2020.

[8] X. Lin, Z. Lin, S. E. Löwenmark, J. Rune, and R. Karlsson, "Doppler shift estimation in 5G new radio non-terrestrial networks," in *IEEE Global Commun. Conf. (GLOBECOM)*, 2021, pp. 1–6.

[9] O. Kodheli, A. Astro, J. Querol, M. Gholamian, S. Kumar, N. Maturo, and S. Chatzinotas, "Random access procedure over non-terrestrial networks: From theory to practice," *IEEE Access*, vol. 9, pp. 109 130–109 143, 2021.

[10] H. Chougrani, S. Kisselef f, W. A. Martins, and S. Chatzinotas, "NB-IoT random access for non-terrestrial networks: Preamble detection and uplink synchronization," *IEEE Internet Things J.*, 2021.

[11] Huawei, HiSilicon, and CAICT, "R1-1908049 Discussion on Doppler compensation, timing advance and RACH for NTN," 3GPP TSG RAN WG1 Meeting #98, Tech. Doc., Aug. 2019.

[12] AT&T, "RP-212729 New WID on IoT NTN enhancements," 3GPP TSG RAN WG1 Meeting #94-e, Tech. Doc., Dec. 2021.

[13] S. Cobb, D. Lawrence, M. O'Connor, G. Gutt, F. Tremblay, and P. Laplante. Test results from an operationally deployed Iridium-based secure timing solution, Satelles, Inc. Accessed: July 9, 2022. [Online]. Available: https://wsts.atis.org/wp-content/uploads/sites/9/2018/11/5-03_Satelles_Cobb_Test-Results-Iridium.pdf

[14] B. Pardhasaradhi, G. Srinath, J. Raghu, and P. Srihari, "Position estimation in indoor using networked GNSS sensors and a range-azimuth sensor," *Inf. Fusion*, vol. 89, pp. 189–197, Jan. 2023.

[15] A. Küpper, *Location-based Services Fundamentals and Operation*. John Wiley & Sons Ltd, 2014.

[16] F. S. Prol, R. M. Ferre, Z. Saleem, P. Välisuo, C. Pinell, E. S. Lohan, M. Elsanhoury, M. Elmusrati, S. Islam, K. Çelikbilek, K. Selv an, J. Yliaho, K. Rutledge, A. Ojala, L. Ferranti, J. Praks, M. Z. H. Bhuiyan, S. Kaasalainen, and H. Kuusniemi, "Position, navigation, and timing (PNT) through low earth orbit (LEO) satellites: A survey on current status, challenges, and opportunities," *IEEE Access*, vol. 10, pp. 83 971–84 002, 2022.

[17] K. Ho and W. Xu, "An accurate algebraic solution for moving source location using TDOA and FDOA measurements," *IEEE Trans. Signal Process.*, vol. 52, no. 9, pp. 2453–2463, 2004.

[18] TR 36.763, "Study on narrow-band internet of things (NB-IoT) enhanced machine type communication (eMTC) support for non-terrestrial networks (NTN)," 3GPP, Tech. Rep., Jan. 2021.

[19] Starlink. Accessed: Nov. 25, 2020. [Online]. Available: https://www.starlink.com/

[20] O. B. Osoro and E. J. Oughton, "A techno-economic framework for satellite networks applied to low earth orbit constellations: Assessing Starlink, OneWeb and Kuiper," *IEEE Access*, vol. 9, pp. 141 611–141 625, 2021.

[21] W. Wang, T. Chen, R. Ding, G. Seco-Granados, L. You, and X. Gao, "Location-based timing advance estimation for 5G integrated LEO satellite communications," *IEEE Trans. Veh. Technol.*, vol. 70, no. 6, pp. 6002–6017, June 2021.

[22] Ericsson, "R1-2005502 On UL time and frequency synchronization enhancements for NTN," 3GPP TSG RAN WG1 Meeting #102-e, Tech. Doc., Aug. 2020.

[23] ——, "R1-1909107 On frequency compensation, uplink timing and random access in NTN," 3GPP TSG RAN WG1 Meeting #98, Tech. Doc., Aug. 2019.

[24] J. A. del Peral-Rosado, R. Raulefs, J. A. López-Salcedo, and G. Seco-Granados, "Survey of cellular mobile radio localization methods: from 1G to 5G," *IEEE Commun. Surveys Tuts.*, vol. 20, no. 2, pp. 1124–1148, 2018.

[25] S. Gezici, Z. Tian, G. B. Giannakis, H. Kobayashi, A. F. Molisch, H. V. Poor, and Z. Sahinoglu, "Localizati on via ultra-wideband radios: a look at positioning aspects for future sensor networks," *IEEE Signal Process. Mag.*, vol. 22, no. 4, pp. 70–84, 2005.

[26] A. C. García, S. Maier, and A. Phillips, *Location-based services in cellular networks: from GSM to 5G NR*. Artech House, 2020.

[27] Qualcomm Incorporated, "R1-161936 NB-PSS and NB-SSS design," 3GPP TSG RAN WG1 NB-IoT Ad-Hoc Meeting, Tech. Doc., Mar. 2016.

[28] Huawei and HiSilicon, "R1-2102344 Discussion on time and frequency synchronization enhancement for IoT in NTN," 3GPP TSG RAN WG1 Meeting #104bis-e, Tech. Doc., Apr. 2021.

[29] TS 38.101-1 V17.8.0, "Evolved universal terrestrial radio access (E-UTRA) user equipment (UE) radio transmission and reception part 1: Range 1 standalone (Release 17)," 3rd Generation Partnership Project (3GPP), Tech. Spec., Jan. 2023.

[30] J. G. Walker, "Satellite constellations," *J. Brit. Interplanetary Soc.*, vol. 37, p. 559, Dec. 1984.

[31] S. W. Paek, S. Kim, and O. de Weck, "Optimization of reconfigurabl satellite constellations using simulated annealing and genetic algorithm," *Sensors*, Feb. 2019.

[32] Huawei and HiSilicon, "R1-1911858 Discussion on performance evaluation for NTN," 3GPP TSG RAN WG1 Meeting #99, Tech. Doc., Nov. 2019.

[33] M. Kleder. WGS84 ellipsoidal earth plotted at 4 pixels per degree, MATLAB central fil exchange. Retrieved: July 4, 2022. [Online]. Available: https://www.mathworks.com/matlabcentral/file xchange/8590- wgs84- ellipsoidal- earth-plotted-at-4-pixels- per-degree

[34] MediaTek and Eutelsat, "R1-2005496 UL time and frequency synchronisation for NR-NTN," 3GPP TSG RAN WG1 Meeting #102-e, Tech. Doc., Aug. 2020.

[35] NORAD GP element sets current data. Accessed: Apr. 19, 2022. [Online]. Available: https://www.celestrak.com/norad/elements/

[36] H. Zhang, Z. Zheng, W.-Q. Wang, and S. Zhang, "Source localisation using TDOA and FDOA measurements under unknown noise power knowledge," *IET Signal Process.*, vol. 14, no. 7, pp. 435–439, Sept. 2020.

[37] R. Amiri, F. Behnia, and A. Noroozi, "An efficien estimator for TDOA-based source localizatio n with minimum number of sensors," *IEEE Commun. Lett.*, vol. 22, no. 12, pp. 2499–2502, 2018.

[38] L. Zhang, T. Zhang, and H.-S. Shin, "An efficien constrained weighted least squares method with bias reduction for TDOA-based localization," *IEEE Sensors J.*, vol. 21, no. 8, pp. 10 122–10 131, 2021.

[39] W. H. Foy, "Position-location solutions by Taylor-series estimation," *IEEE Trans. Aerosp. Electron. Syst.*, vol. AES-12, no. 2, pp. 187–194, 1976.

[40] B. Jin, X. Xu, and T. Zhang, "Robust time-difference-of-arrival (TDOA) localization using weighted least squares with cone tangent plane constraint," *Sensors*, vol. 18, no. 3, 2018.

[41] X. Jin-yu, W. Wei, and Z. Zhong-liang, "A new TDOA location technique based on Taylor series expansion in cellular networks," in *Proc. 4th Int. Conf. Parallel Distrib. Comput. Appl. Technol.*, 2003, pp. 378–381.

[42] N. Levanon, "Quick position determination using 1 or 2 LEO satellites," *IEEE Trans. Aerosp. Electron. Syst.*, vol. 34, no. 3, pp. 736–754, 1998.

[43] K. Shamaei, J. Khalife, and Z. M. Kassas, "Exploiting LTE signals for navigation: Theory to implementation," *IEEE Trans. Wireless Commun.*, vol. 17, no. 4, pp. 2173–2189, 2018.

[44] F. Guo, Y. Fan, Y. Zhou, C. Xhou, and Q. Li, *Space Electronic Reconnaissance: Localization Theories and Methods*. Wiley Telecom, 2014.

[45] Qualcomm Incorporated, "R1-1802324 Reduced system acquisition time," 3GPP TSG RAN WG1 Meeting #92, Tech. Doc., Mar. 2018.

[46] K. Ota, A. Shimura, M. Sawahashi, and S. Nagata, "Performance of physical cell ID detection probability considering frequency offset for NR radio interface," in *IEEE 90th Veh. Technol. Conf. (VTC2019-Fall)*. IEEE, 2019, pp. 1–6.

[47] I. Céspedes, Y. Huang, J. Ophir, and S. Spratt, "Methods for estimation of subsample time delays of digitized echo signals," *Ultrason. Imag.*, Apr. 1995.

[48] J. He and H. C. So, "A hybrid TDOA-fingerprinting-base localization system for LTE network," *IEEE Sensors J.*, vol. 20, no. 22, pp. 13 653–13 665, Nov. 2020.

[49] MCC Support, "Final report of 3GPP TSG RAN WG1 #107-e v1.0.0," Jan. 2022.

[50] R. J. Carroll, C. F. J. Wu, and D. Ruppert, "The effect of estimating weights in weighted least squares," *J. Amer. Statist. Assoc.*, vol. 83, no. 404, pp. 1045–1054, 1988.

[51] O. Liberg, M. Sundberg, E. Wang, J. Bergman, and J. Sachs, *Cellular Internet of Things Technologies, Standards, and Performance*. Academic Press, Sept. 2017.

[52] TS 36.133 V17.6.0, "Evolved universal terrestrial radio access (E-UTRA) requirements for support of radio resource management (Release 17)," 3rd Generation Partnership Project (3GPP), Tech. Spec., June 2022.

[53] S. M. Kay, *Fundamentals of statistical signal processing: Estimation theory*. Prentice Hall, 1993.

[54] S. Stein, "Algorithms for ambiguity function processing," *IEEE Trans. Acoust., Speech, Signal Process.*, vol. 29, no. 3, pp. 588–599, June 1981.

[55] Z. Şahinoğlu, S. Gezici, and I. Güvenç, *Ultra-wideband Positioning Systems: Theoretical Limits, Ranging Algorithms, and Protocols*. Cambridge University Press, 2008.

[56] Y. Qi and H. Kobayashi, "An optimum positioning receiver for nonsynchronized mobile systems," in *Proc. 37th Annu. Conf. Inf. Sci. Syst.*, Mar. 2003.

[57] TS 24.008 V18.1.0, "Mobile radio interface layer 3 specification core network protocols; stage 3 (Release 18)," 3rd Generation Partnership Project (3GPP), Tech. Spec., Dec. 2022.

[58] Y. Shi, "Power saving methods for LTE-M and NB-IoT devices," White Paper, Rhode & Schwarz, June 2019.

[59] TS 36.331 V17.3.0, "Evolved universal terrestrial radio access (E-UTRA) radio resource control (RRC) protocol specificatio (Release 17)," 3rd Generation Partnership Project (3GPP), Tech. Spec., Jan. 2023.

[60] TR 38.913 V17.0.0, "Study on scenarios and requirements for next generation access technologies (Release 17)," 3rd Generation Partnership Project (3GPP), Tech. Rep., Apr. 2022.

[61] MediaTek, "R1-2103962 Summary #3 of AI 8.15.1 Scenarios applicable to NB-IoT/eMTC," 3GPP TSG RAN WG1 Meeting #104bis-e, Tech. Doc., Apr. 2021.

[62] Y. Su, Y. Liu, Y. Zhou, J. Yuan, H. Cao, and J. Shi, "Broadband LEO satellite communications: architectures and key technologies," *IEEE Wireless Commun.*, vol. 26, no. 2, pp. 55–61, 2019.

[63] K. Scarbrough, R. J. Tremblay, and G. C. Carter, "Performance predictions for coherent and incoherent processing techniques of time delay estimation," *IEEE Trans. Acoust., Speech, Signal Process.*, vol. 31, no. 5, pp. 1191–1196, Oct. 1983.

[64] K. L. Bell, Y. Steinberg, Y. Ephraim, and H. L. Van Trees, "Extended Ziv-Zakai lower bound for vector parameter estimation," *IEEE Trans. Inf. Theory*, vol. 43, no. 2, pp. 624–637, Mar. 1997.

[65] *Product Specification*, nRF9160, Nordic Semiconductor, Oct. 2021, v2.1.

[66] *Cellular IoT Module with BLE*, AES-CELLIO T-AVT9152MOD, Avnet, July 2021, rev 1.1.

[67] R. Fasthuber, F. Catthoor, P. Raghavan, and F. Naessens, *Energy-Efficient Communication Processors: Design and Implementation for Emerging Wireless Systems*. Springer, 2013.